UNIVERSITY OF CALIFORNIA

Los Angeles

Effects of Morphology on the Reaction Kinetics of Calcium Oxide Carbonation

A thesis submitted in partial satisfaction

of the requirements for the degree Master of Science

in Chemical Engineering

by

Derrick Rosales

2017

ABSTRACT OF THE THESIS

Effects of Morphology on the Reaction Kinetics

of Calcium Oxide Carbonation

by

Derrick Rosales

Master of Science in Chemical Engineering

University of California, Los Angeles, 2017

Professor Dante A. Simonetti, Chair

A foundation for the analysis of chemical reactions using thermogravimetric analysis is presented here. Calcium oxide has been shown to be invaluable in steam-methane reform processes due to its ability to pick up and sequester carbon dioxide. Calcium oxide derived from marble, calcium acetate, and electrospun composite nanofibers are carbonated in a thermogravimetric analyzer at various temperatures. Generally, a larger conversion of calcium oxide to calcium carbonate was reached at higher temperatures. For the marble precursor, the conversion increased from 40% at 600°C to 66% at 800°C under an atmospheric pressure of 100% CO_2. The conversion trends are compared and contrasted between the precursors. A study on the effect of sample age and sample pretreatments was conducted, which showed that sample age slightly affected

carbonation kinetics by increasing peak reaction rate of a marble-derived sample from 0.07 mol/min to 0.10 mol/min. Multiple pretreatments seemed to have no effect on conversion nor reaction rates. The electrospun composite nanofibers outperformed the other precursors across all temperatures, reaching complete conversion at 650°C, while the marble-derived sample only reached 41%, and the calcium acetate-derived sample only reached 84%. By applying the random pore model and the overlapping grain model to these conversion trends, kinetic rate constants and diffusivities can be estimated, providing a quantitative method to compare and contrast sorbent performance, With this method, the marble-derived sample was shown to exhibit poor performance, with a kinetic rate constant of 2.6×10^{-4} $cm^2/mol/s$ compared to the nanofiber's 5.6×10^{-4} $cm^2/mol/s$ at 650°C.

The thesis of Derrick Rosales is approved.

Panagiotis D. Christofides

Vasilios Manousiouthakis

Dante A. Simonetti, Committee Chair

University of California, Los Angeles

2017

Table of Contents

List of Figures

List of Tables

Notation

Notation: Latin

a_i	Fraction of solid particles of the i'th grain size
C_b	Bulk concentration of gaseous phase (mol/L)
C_e	Equilibrium concentration of gaseous phase (mol/L)
D_{OGM}	Diffusion coefficient based on OGM (m^2/s)
D_{RPM}	Diffusion coefficient based on RPM (m^2/s)
k_{OGM}	Rate constant of OGM (m/s)
k_{RPM}	Rate constant based on RPM ($m^4/mol/s$)
L_0	Initial total length of pore system per unit volume (m/m^3)
M_{CaO}	Molar weight of calcium oxide (g/mol)
M_{CO_2}	Molar weight of carbon dioxide (g/mol)
r	Radius of reactive pore (m)
$r_{0,i}$	Initial radius of reactive core and grain (m)
$r_{c,i}$	Radius of reactive core of i'th grain size (m)
$r_{g,i}$	Radius of grain of i'th grain size (m)
S_0	Initial surface area of pore system per unit volume (m^2/m^3)
t	Time (s)
$v_0(r)$	Pore size distribution of material (1/m)
V_{CaO}	Molar volume of calcium oxide (m^3/mol)
W_0	TGA reading of initial sample weight before carbonation (g)
W_t	TGA reading of sample weight at time t (g)
X	Conversion
Z	Molar ratio of product to reactant

Notation: Greek

β	Modified Biot number
ε_0	Initial porosity of sorbent
$\varepsilon_{c,i}$	Porosity of reactive cores of the i'th grain size
$\varepsilon_{g,i}$	Porosity of the sorbent grains of the i'th grain size
ρ_{CaO}	Bulk density of calcium oxide
Ψ	Structural parameter for use in the RPM

Background

Hydrogen is an important commodity chemical that is used for a variety of purposes, from synthesizing ammonia to fueling vehicles. Traditionally, large amounts of hydrogen are manufactured in steam methane reforming plants, in which steam and methane are fed into a reformer to yield carbon monoxide and hydrogen. Furthermore, the resulting carbon monoxide can react with steam to produce carbon dioxide and more hydrogen. The steam methane reforming (SMR) and water-gas shift (WGS) reactions are presented below.

$$CH_4 + H_2O \rightarrow CO + 3H_2 \quad (1)$$

$$CO + H_2O \rightarrow CO_2 + H_2 \quad (2)$$

$$CH_4 + 2H_2O \rightarrow CO_2 + 4H_2 \quad (3)$$

The hydrogen then undergoes various compression steps, depending on the process, for transportation. These compression steps may include pressure swing adsorption, to purify the product stream (Barelli, Bidini et al. 2008). Because of the endothermic nature of the SMR reaction, a large amount of energy has to be supplied to the reactor. In addition to this energy cost, due to the discrepancy between the enthalpies of each reaction, the SMR reactor is followed by a series of high temperature shift and low temperature shift reactors, so the WGS reaction can take place. Typically, the SMR, WGS, and purification stages are done in multiple, separate unit operations. These processes operate at varying temperatures (800°C-1000°C) and pressures (14-20 atm), leading to a large capital cost of the construction and operation of this process (Barelli, Bidini et al. 2008).

One technique to alleviate the costs is to sequester the produced carbon dioxide from the WGS reaction. This sorption enhanced steam methane reform (SE-SMR) reaction will push the

equilibrium towards more hydrogen production. It has also been shown that the multistage production of hydrogen can be simplified into a single stage system, while maintaining comparable hydrogen production (Albrecht, Satrio et al. 2010). This sorption enhanced system is not without its drawbacks however, as the best performing sorbent, calcium oxide, is subject to quick loss of activity over only a few cycles (Grasa and Abanades 2006). In addition to this, conversion is highly limited by intra-particle mass transfer diffusion considerations due to a formation of a calcium carbonate shell, which develops after the kinetically controlled regime ends (Bhatia and Perlmutter 1983). To combat these phenomena, it is theorized that employing electro spun nanofibers will provide a system in which the sorbent is in close molecular proximity to the catalytic sites, therefore assisting in the carbon dioxide sequestration.

Electrospun nanofibers have shown promise in the catalysis field (Thavasi, Singh et al. 2008). With a high surface-to-area ratio and large intra-fiber void volumes, nanofibers have great potential to be effective catalysts for methane conversion, possibly sporting higher conversions and increased stability. By utilizing composite metal-oxide nanofibers, perhaps the benefits of calcium oxide based sorbents will not be overshadowed by their limitations.

The work presented here will focus on the sequestration of carbon dioxide from the steam methane reforming system. Characterization of the traditional calcium oxide sorbents, obtained from various precursors, will be compared to the electrospun nanofibers. The reaction of interest, the conversion of calcium oxide to calcium carbonate, will also be compared across the sorbents. By analyzing both the kinetically and mass transfer controlled regimes of carbonation, a more complete understanding of the underlying microkinetic phenomena can be achieved. Existing mathematical models derived from the physical nature and geometry of the sorbents describe catalytic activity, and can be applied to this sorption system, providing a basis for comparing and

contrasting sorbents quantitatively. The validity of these physical models and their usefulness will be explored as well. Combining the knowledge of the physical and chemical properties of the carbonation sorbents will allow for the building of accurate process models and parameters that can be utilized to determine if SE-SMR systems with nanofibers are more economical than traditional SE-SMR systems.

Introduction

A deeper kinetic understanding of sorbent technology and CO_2 capture can be applied across many different industries and sectors, especially in today's environmentally-conscious academic climate. In addition to the potential environmental benefits of advancing CO_2 capture technology, a large motivator for this research is to enhance the traditional SMR systems and increase hydrogen production efficiency. As mentioned earlier, traditional SMR is a complex, multistep process that is operated at varying temperatures (>800°C, 300°C to 400°C, 200°C) and with different catalysts (nickel to iron oxide/chromium oxide to copper-zinc oxide) at each step (Albrecht, Satrio et al. 2010). As one of the products of the methane reforming reaction is CO_2, its capture and removal from the reaction rig will push the equilibrium towards increased hydrogen production. Many studies have been done to determine a good candidate for CO_2 capture, but calcium oxide based materials are the most attractive due to their high reactivity, high capacity, and low material cost (Li, Fang et al. 2012). Not only is the carbonation behavior of calcium oxide attractive, the addition of a calcium oxide sorbent in the reaction system is also thermodynamically beneficial. By introducing the calcium oxide carbonation reaction to the SMR and WGS reactions presented above, the magnitude of the difference in enthalpy for the overall reaction system

decreases. This allows for the simplification of the complex multistep process into a single unit operation that can produce comparable hydrogen production.

$$CH_4 + H_2O \rightarrow CO + 3H_2 \quad (4)$$

$\Delta H_{25°C}$ = 210 kJ/mol

$$CO + H_2O \rightarrow CO_2 + H_2 \quad (5)$$

$\Delta H_{25°C}$ = -42 kJ/mol

$$CaO + CO_2 \rightarrow CaCO_3 \quad (6)$$

$\Delta H_{25°C}$ = -175 kJ/mol

Previous work has shown that as expected, both thermodynamic simulations and experimental results indicate greater hydrogen production when the system contains a sorbent, across a wide range of temperatures and pressures (Albrecht, Satrio et al. 2010). For example, at a reaction temperature of 650°C, hydrogen equilibrium concentration was about 95% for a system with CO_2 sorption, compared to about 75% for a system without (Albrecht, Satrio et al. 2010).

As mentioned earlier, calcium oxide sorbents have the unfortunate disadvantage of loss of activity over multiple carbonation and calcination cycles. Because the long term goal of this calcium oxide carbonation study is to improve large-scale hydrogen production processes, this loss of activity is economically detrimental. At a molecular level, this degradation is explained by three phenomena that occur during a typical carbonation/calcination cycle: (1) Because the calcium oxide carbonation reaction is highly exothermic (as indicated above), the temperature of the reaction area increases greatly during carbonation, leading to severe sintering and pore clogging

of the sorbent; (2) As CaO converts to $CaCO_3$, its volume increases, causing the distance between individual carbonated particles to decrease, which makes for a cramped system that is more susceptible to sintering; (3) The energy of the $CaCO_3$ particles becomes large enough to significantly affect sorbent morphology at 533°C, which is lower than the typical reaction temperatures SMR is traditionally performed at (Li, Fang et al. 2012).

A multitude of methods have been employed in an attempt to increase the lifespan of the sorbent. Research labs have supported the calcium oxide with more robust metals such as magnesium oxide, in a physically mixed system, which seemed to decelerate the sorbent degradation (Li, Fang et al. 2012). Other groups have attempted to support the sorbent by coating it with a strong, porous alumina shell (Albrecht, Satrio et al. 2010). Synthetic blends of wet-mixed calcium oxide and aluminum oxides have also been studied, in which these sorbents performed well, with comparable activities and increased stability (Liu, Dennis et al. 2012, Zhou, Xu et al. 2013). Adding these inert supports seemed to have been somewhat successful, as they prolonged the lifespan of the calcium oxide sorbent while maintaining the required activity. However, the addition of these materials increases the overall cost of the process, which takes away from the attractive low-cost feature of calcium oxide. A different approach taken to solve this problem has been researched as well. It has been seen that hydrating sorbents that have been carbonated and calcined ten times in a pressurized reactor led to significantly higher carbonation degree (Manovic and Anthony 2007). Interestingly enough, this steam hydration even led to carbonation degrees larger than fresh, un-cycled sorbent (Manovic and Anthony 2007). While a promising technique, this method requires an additional steam hydration unit operation, which will incur a large increase in utility and operating costs, especially for large scale processes.

Polymer nanofibers are a novel material whose properties have applicability in many different fields. Because of their nano-scale, polymer nanofibers have a large surface area to volume ratio, a wide range of flexibility, and strong mechanical stability (Huang, Zhang et al. 2003). Synthesis techniques include drawing, template synthesis, phase separation, self-assembly, and electrospinning. However, electrospinning shows the greatest potential for scale-up for industrial mass production (Huang, Zhang et al. 2003). The creation of electrospun polymer nanofibers is relatively simple, as it only requires a voltage, a polymer solution being fed by a syringe, and a metal collection surface. A high voltage is applied between the syringe tip and the metal collection surface, which induces a charge on the surface of the polymer solution, as it experiences oppositng electrostatic forces and surface tension (Huang, Zhang et al. 2003). These counteracting forces cause the deformation of the liquid into a conical shape, called the Taylor cone, and as the electrostatic forces are increased and reach a breaking point, liquid is dispensed from the syringe tip (Huang, Zhang et al. 2003). As the liquid travels through the air, the solvent evaporates, leaving only the charged elongated polymer. This polymer then collects on the metal surface.

This electrospinning process presents an interesting parameter optimization problem, as many inputs are required to produce these fibers, which will affect the physical and chemical properties of the product. Voltage, polymer travel path length, solution properties and constituents, syringe flow rates, and many more input parameters can be studied to achieve efficient, effective, and economical nanofiber production. Extensions to this method can also be made by introducing more parameters, such as controlling the electrospinning chamber humidity, or even the addition of metal oxides into the polymer solution formulation. The addition of metals into the electrospinning formula is important in the catalytic industry, as nanofiber technology shows

potential. It has been shown that coating electrospun nanofibers with platinum nanoparticles to create platinum nanowires produces a catalytic system with high activity (Formo, Lee et al. 2008). In fuel cells, nanofibers are being studied as a platinum catalyst support, as the even dispersion of platinum onto the fibers and polymer stability present attractive features that may reduce overall platinum usage (Thavasi, Singh et al. 2008).

To glean potentially useful kinetic information for the carbonation reaction system presented, a method must be developed to measure the extent of conversion and carbonation. A thermogravimetric analyzer will be employed to study this gas-solid adsorbent reaction, in which a solid phase consisting of solid sorbent will be surrounded by flowing gas containing the material to be adsorbed. Mass readings will be taken, which can then be manipulated to calculate calcium oxide conversion and reaction rates. Physical models taken from literature can then be applied to the experimental conversion data to estimate parameters. A characteristic feature of this carbonation reaction is its distinct separation of two stages. The first stage is a fast, kinetically controlled stage in which carbonation occurs rapidly, before suddenly transitioning into a slower, less rapid diffusion controlled stage (Li, Fang et al. 2012). Previous work has shown that calcium oxide derived from various precursors are structurally different, and as such, vary wildly in their performance as a sorbent (Lu, Reddy et al. 2006). It is well known that calcium oxide derived from calcium acetate (CaO-CaAcetate) experiences a much larger conversion than calcium oxide derived from geographical sources, such as marble or limestone (Silaban, Narcida et al. 1992). This phenomena will be studied here, as vendor supplied calcium oxide derived from marble (CaO-Marble) will be compared to calcium oxide derived from calcium acetate. These two samples will then be compared to calcium oxide derived from electrospun nanofibers (CaO-NF). To further supplement this data, a temperature study will also be conducted on these three

precursors of calcium oxide, as other research groups have shown that increasing temperature increases the extent of carbonation (Li, Fang et al. 2012).

Experimental

Thermogravimetric analysis was conducted with a Perkin Elmer TGA system. There are two gas inlets, which were usually reserved for argon and CO_2. These inlets feed into rotameters, which are manually adjusted to change the gas flow rate. The sample pan and a reference pan are suspended atop pan holders inside the TGA furnace, while gas flows through them. The reference pan is to provide a buoyancy correction to compensate for the effect of temperature on the gases flowing through the pans. Alumina crucibles were used to hold the sample. Temperatures ranged from 600°C-800°C, and were attained with a scanning rate of 20°C/min. Gas flow rates were set at 200 ml/min, in an attempt to minimize external diffusion from the bulk gas to the sample interface.

CaO-Marble was pretreated in an open air oven at 650°C at a ramp rate of 5°C/min, for 8 hours. To create CaO-CaAcetate, calcium acetate was converted to calcium carbonate and then calcium oxide in an open air oven at 750°C at a ramp rate of 5°C/min for 8 hours. Both samples were then crushed and sieved to 200 mesh, and the fines were used for the experiments. A mesh of 200 corresponds to particle sizes smaller than 75 μm. This was done to ensure consistency between runs, however previous work indicates that particle size of the sorbent had almost no effect on the carbonation behavior (Zhou, Xu et al. 2013).

CaO-NF was prepared by the electrospinning method described above. The polymer solution consisted of 1.3 g of PVP dissolved in 20mL of ethanol mixed with 0.975 g of CaO-Marble dissolved in 10mL of DI water. This solution was then loaded into a 30 mL plastic syringe.

A 30 kV voltage was applied between a 16 inch distance between the needle tip and the metal collection surface. An air flow rate of 6 sccm into the electrospinning chamber was employed to ensure constant humidity conditions. To create the nanofibers, the polymer solution was excreted at a flowrate of 1 mL/hr, and was then collected on the metal plate. These brown-colored, tissue-like nanofibers were then treated in an open air oven at 500°C, and again at 650°C for eight hours at a ramp rate of 5°C/min to ensure the full removal of any remaining PVP and other unwanted constituents. This higher temperature was chosen as it is greater than 550°C, the temperature at which equilibrium CO_2 in the air is greater than the equilibrium CO_2 in calcium oxide. After these pretreatment steps, the remaining sample was a white powder.

A typical run consisted of loading 3-16 mg of sample into the TGA, and then heating up to the specified reaction temperature at a rate of 20°C/min under argon. The wide discrepancy of initial sample weights is due to the inherent differences in the three different samples' bulk densities. In each run, the sample pan was filled with about the same volume of sample, and the CaO-Marble reached about 16 mg, while the CaO-CaAcetate sample reached about 9 mg, and the CaO-NF reached about 3 mg. The TGA records the sample's mass and temperature, taking a data point every second. Once the reaction temperature is reached, an additional waiting time is necessary to ensure that the mass has stabilized. During this period of time in which the temperature is steadily increasing, any adsorbed water or CO_2 from ambient conditions are burned off. Once mass has stabilized to an acceptable value, a software command allows for the switching of gases, from argon to pure CO_2 to start the carbonation. This carbonation then usually takes place for about an hour before the run is stopped and the TGA begins to cool. From the raw mass data, conversion can be calculated by the following formula:

$$X = \frac{W_t - W_0}{W_0} * \frac{M_{CaO}}{M_{CO_2}} \quad (7)$$

In the equation above, W_t and W_0 are the weight reading at a time t, and initially, while M_{CO_2} and M_{CaO} are the molecular weights of CO_2 and CaO, respectively. Also from this exported TGA data, normalized reaction rates can be calculated, given by:

$$reaction\ rate = \frac{W_t - W_0}{t_n - t_{n-1}} * \frac{M_{CaO}}{M_{CO_2}} * \frac{1}{W_0} \quad (8)$$

These conversion trends were then inputted into Athena, a differential equation solver and parameter estimating software. Once the physical models have been built in Athena, the software can compare its modeled results to the conversion trends, allowing for the estimating of the reaction rate coefficients and the diffusivities of the material.

To better quantify the analysis of this sorption system, physical models derived from the geometry of the reaction site can be applied. Within these models, useful parameters can be estimated, leading to a more quantitative method of differentiating the reactive activities of various catalysts or materials. In this case, the models will be applied to the various calcium oxide precursors. Two models will be studied here: (1) The Random Pore Model, in which the surface area of the pores are the reactive sites, and (2) the Overlapping Grain Model, in which the material is assumed to consist of spherical, overlapping grains that react with the gaseous phase with its exposed surface area.

The Random Pore Model (RPM) was first proposed by S.K. Bhatia and D.D. Perlmutter, in an attempt to successfully capture the effect of a materials' pore size distribution in fluid-solid

reactions. Compared to prior models based on grain geometry or order-of-reaction models, the RPM provides more flexibility as it realizes that reaction rate decreases that occur in the later stages of a reaction are due to the intersections of growing, non-reactive product surfaces (Bhatia and Perlmutter 1980). In addition to this, the RPM allows for a distribution of pore sizes, which creates a much more accurate model, compared to older models that assumed a uniform grain size (Bhatia and Perlmutter 1981). These non-reactive product surfaces serve as a diffusional barrier that the fluidic phase must diffuse through in order to react. In the initial stages of a reaction, the kinetic regime dominates and accounts for almost all of the reaction rate. As the non-reactive product surfaces grow and intersect with each other, the system transitions into a more diffusion dominated regime.

Assuming that the pores are cylindrical and are not created nor destroyed, an expression encompassing both the kinetically controlled and the diffusion controlled regimes can be written as follows (Bhatia and Perlmutter 1980, Bhatia and Perlmutter 1981).

$$\frac{dX}{dt} = \frac{k_{RPM} S_0 C_b (1-X)\sqrt{1-\Psi ln(1-X)}}{(1-\varepsilon_0) * \left(1 + \beta \frac{Z}{\Psi}\left[\sqrt{1-\Psi\, ln(1-X)} - 1\right]\right)} \quad (9)$$

Within **Equation 9**, the Z term is the ratio of the molar volume of the product to the molar volume of the reactants. The β term represents a modified Biot number that encompasses the rate constant and the effective product layer diffusivity of the system at hand. For a stoichiometrically balanced equation, such as the carbonation of calcium oxide, this Biot number can be expressed as (Bhatia and Perlmutter 1981, Bhatia and Perlmutter 1983).

$$\beta = \frac{2k_{RPM}(1-\varepsilon_0)}{V_{CaO}D_{RPM}S_0} \quad (10)$$

The parameter Ψ is a function of three structural parameters that can be calculated from a pore size distribution of the material, $v_0(r)$, typically obtained by mercury porosimetry. These parameters are S_0, the initial surface area of reaction, L_0, the initial total length of pore structure, and ε_0, the initial porosity, and can be calculated as follows (Grasa, Murillo et al. 2009):

$$S_0 = \int_0^\infty \frac{2v_0(r)}{r}\,dr \quad (11)$$

$$L_0 = \int_0^\infty \frac{v_0(r)}{\pi r^2}\,dr \quad (12)$$

$$\varepsilon_0 = \int_0^\infty v_0(r)dr \quad (13)$$

$$\Psi = \frac{4\pi L_0(1-\varepsilon_0)}{S_0^2} \quad (14)$$

In the kinetic region, the modified Biot number tends to 0, and in the diffusion region, the modified Biot number tends to infinity. Applying this to **Equation 10**, and then integrating and simplifying the resulting **Equation 9** allows for the creation of two distinct functions relating conversion and time (Grasa, Murillo et al. 2009). In the kinetic region, **Equation 9** can be simplified to **Equation 15**.

$$\frac{dX}{dt} = \frac{k_{RPM} S_0 C_b (1-X)\sqrt{1-\Psi ln(1-X)}}{(1-\varepsilon_0) * (1)} \quad (15)$$

Then, by using separation of variables, the resulting equation can be integrated from zero to unity with the initial condition that conversion is zero at time equals zero.

$$\int \frac{1}{(1-X)\sqrt{1-\Psi ln(1-X)}} dX = \int \frac{k_{RPM} S_0 C_b}{(1-\varepsilon_0)} dt \quad (16)$$

$$\frac{2\sqrt{1-\Psi \ln(1-X)}-1}{\Psi} = \frac{k_{RPM} S_0 (C_b - C_e) t}{(1-\varepsilon_0)} \quad (17)$$

A similar technique can be used for the diffusion controlled region. In this case, **Equation 9** can be simplified to **Equation 18**.

$$\frac{dX}{dt} = \frac{2 S_0^2 C_b \rho_{CaO} (1-X)\sqrt{1-\Psi ln(1-X)}}{D_{RPM} M_{CaO} (1-\varepsilon_0)^2 * \left(\frac{1}{\Psi}\left[\sqrt{1-\Psi\, ln(1-X)}-1\right]\right)} \quad (18)$$

By separation of variables, the resulting equation can also be integrated from zero to unity with the initial condition that conversion is zero at time equals zero.

$$\int \frac{\frac{1}{\Psi}\left[\sqrt{1-\Psi\, ln(1-X)}-1\right]}{(1-X)\sqrt{1-\Psi ln(1-X)}} dX = \int \frac{2 S_0^2 C_b \rho_{CaO}}{D_{RPM} M_{CaO} (1-\varepsilon_0)^2} dt \quad (19)$$

Now, both **Equation 17** and **Equation 19** can be rearranged for ease of use, into **Equation 20** and **Equation 21**.

$$\frac{1}{\Psi}\left[\sqrt{1-\Psi\, ln(1-X)}-1\right]=\frac{k_{RPM}S_0(C_b-C_e)t}{2(1-\varepsilon_0)} \quad (20)$$

$$\frac{1}{\Psi}\left[\sqrt{1-\Psi\, ln(1-X)}-1\right]=\frac{S_0}{1-\varepsilon_0}\sqrt{\frac{D_{RPM}M_{CaO}C_b t}{2\rho_{CaO}Z}} \quad (21)$$

The left hand side of **Equation 20** and **Equation 21** represents a modified conversion which conveniently sports a simple algebraic relation to the useful parameters k_{RPM} and D_{RPM}. In the kinetically controlled region, the modified conversion is linearly proportional to time, while in the diffusion limited case, modified conversion has a square root of time dependence. **Equation 20** and **Equation 21** will be fitted to experimental data to extract and estimate the kinetic rate constants and diffusivities of various precursors at various temperatures. An additional caveat to this system is the addition of a third parameter. The optimal "switch time" will also be estimated, in which the software will choose a time to switch from **Equation 20** to **Equation 21**, such that the square of the residuals between the modeled and observed conversions are minimized. This allows for the elimination of a static arbitrary kinetic period cutoff time that may convolute the estimated parameters k_{RPM} and D_{RPM}.

Values from literature can be used as a basis for the model parameters present within the RPM for the purpose of parameter estimation. These values describe the pore structure of the material at hand. For CaO-Marble, these structural parameters were assumed to be identical, or at least similar, to structural parameters presented for calcium oxide derived from Imeco limestone,

a type of limestone from Spain (Grasa, Murillo et al. 2009). Geophysically, marble is a metamorphosed form of limestone, which is a sedimentary rock. However, the main constituent in both marble and limestone is calcium carbonate, and the values presented for Imeco limestone will provide a comparable approximation of marble's structural parameters for the purposes of modeling the system.

For CaO-CaAcetate, the pore size distribution $v_0(r)$ was extrapolated from previous work that provided this data (Lu, Reddy et al. 2006). From this distribution, the area under the curve can be estimated using rough Riemann sums, which allows for the calculation of the other structural parameters S_0, L_0, and ε_0 from **Equations 11-14**. These values can then be used to calculate Ψ. While no information detailing the pore size distribution of CaO-NF is present in the literature, the structural parameters can be approximated to provide a suitable model for the purposes of comparison. To estimate these parameters, it is assumed that the CaO-NF structural parameters are similar to the CaO-Marble from which they were synthesized from. Taking this into account, the CaO-NF porosity was approximated to be slightly larger than the calculated CaO-CaAcetate porosity, and the S_0 and L_0 were approximated to be 5% larger than the CaO-Marble. In all three of the precursors, a more accurate representation of the system's actual structural parameters can be achieved by conducting mercury porosimetry on the samples. However, these values taken from the literature and estimated from similar materials provide suitable approximations for the samples, and can still be used to quantitatively compare the samples' performances using parameter estimation. The structural parameters for the three sorbents are provided in **Table 1**.

Table 1. Structural parameters for three calcium oxide precursors for use in the RPM. Marble values are taken from the literature, while Calcium Acetate values were calculated from a pore size distribution curve. Nanofiber values were guessed to be similar, but slightly larger, than their marble precursor counterpart.

Precursor	Structural Parameter			
	S_0 (m^2/m^3)	L_0 (m/m^3)	ε_0	Ψ
Marble	4.2×10^7	4.2×10^{14}	0.47	1.57
Calcium Acetate	1.9×10^7	5.7×10^{13}	0.68	0.634
Nanofibers	4.4×10^7	4.4×10^{14}	0.70	0.847

The Overlapping Grain Model (OGM) is based upon the assumption that the sorbent is made up of solid spheres, in which product forms and accumulates on the surface causing the overall grain to grow while its reactive core shrinks (Liu, Dennis et al. 2012). As with the RPM, the gaseous phase must diffuse across this product barrier. However in the OGM, the product layer is on the outside of a spherical grain, instead of the inside surface area of a pore. The OGM is robust enough to account for various discrete grain sizes that may be found in the sorbent, and it also accounts for the extent of their overlap due to the growth of the product layer (Liu, Dennis et al. 2012). For each discrete grain size, two differential equations must be employed: one describing rate of change of volume of the core, and of the grain itself. Before any reaction has occurred and any product layer has formed, the volume of the core and the grain are equal. What results is a mixed system of three algebraic equations and two differential equations per discrete grain size.

By applying a molar and volume balance to the system, two differential equations can be derived describing the rate of core shrinkage and rate of grain growth, with the subscript i denoting a specific grain size (Liu, Dennis et al. 2012):

$$\frac{dr_{c,i}}{dt} = -\frac{V_{CaO} D_{OGM} (C_b - C_e)}{r_{c,i}\left[1 - \left(\frac{r_{c,i}}{r_{g,i}}\right)\right] + \left(\frac{D_{OGM}}{k_{OGM}}\right)} \quad (22)$$

$$\frac{dr_{g,i}}{dt} = -\frac{dr_{c,i}}{dt}\left[(Z-1)\frac{\varepsilon_c}{\varepsilon_g}\frac{r_{c,i}^2}{r_{c,i}^2}\right] \quad (23)$$

Furthermore, the core porosity ε_c can be calculated and expressed in terms of a single reactive core radius by applying derived relationships, which can then be used to calculate the porosity of the grains ε_g by conducting a volume balance (Avrami 1940, Sotirchos 1987, Liu, Dennis et al. 2012).

$$\varepsilon_c = \exp\left[\ln(\varepsilon_0)\sum \frac{a_i r_{c,i}^3}{r_{0,i}^3}\right] \quad (24)$$

$$\varepsilon_g = \varepsilon_0 - (Z-1)(\varepsilon_c - \varepsilon_0) \quad (25)$$

Lastly, the local conversion can be calculated by conducting a molar balance (Sotirchos and Yu 1988).

$$X = \frac{\varepsilon_0 - \varepsilon_g}{(Z-1)(1-\varepsilon_0)} \quad (26)$$

Equations 22-26 were solved in a differential equation solver, and **Equation 26** was fit to experimental data. From this model, just as with the RPM, kinetic rate constants and diffusivities of various precursors of calcium oxide and at various temperatures can be estimated using software. The only parameters required for the OGM is the initial porosity and the grain size

distribution. The initial porosities of the sorbents have been listed in **Table 1**. It has been shown that using image analysis software on SEM images of the sorbent can provide a decent approximation for the grain size distribution (Liu, Dennis et al. 2012). However, the porosity and the grain size distribution presented for a synthetic CaO-based sorbent will be used here, for the purposes of demonstrating the ability to estimate parameters using the OGM. This discrete grain size distribution is listed in **Table 2**, with $r_{0,i}$ and a_i representing the initial grain size radius and the fraction of solid particles of that grain size, respectively. These values will be employed for all three of the studied precursors.

Table 2. Discrete grain size distribution of a synthetic CaO-based sorbent that will be employed here. Values were taken from literature, in which they were calculated using image analysis software ran on SEM images of the sorbent used.

$r_{0,i}$ (nm)	a_i
50	0.40
100	0.30
200	0.15
400	0.10
800	0.05

Results and Discussion

Results and Discussion: TGA Functionality

Preliminary tests were run on the TGA system to validate its function, accuracy, and repeatability. A drift test was conducted by placing a blank reference and sample pan into the instrument and simply measuring its differential mass change under 200 mL/min of argon. After a set amount of time, the gas would be switched to pure CO_2 at 200 mL/min to emulate run

conditions. To get a general idea of the magnitude of instrument drift that may be experienced during experimental runs, mass change was measured at room temperature, and during a ramp rate of 20°C/min to 670°C. Results indicated the gas switching process did affect mass slightly, and that a higher temperature did induce a larger drift. However, both mass deviations are small enough such that conversion results will not be compromised. Because the pans are ~140 mg, and the samples ranged from 3-16 mg, the drift from the blank pans should be representative of the drift experienced during an experimental run. From **Figure 1**, it can be seen that the blank alumina pans drifted about 0.03mg at room temperature, after one hour under argon and one hour under CO_2. Under argon, there was almost no drift, however the sample began to drift after the switch to the CO_2. At 670°C, a more prominent drift of 0.2 mg was observed, with about half of the drift occurring during the ramp portion of the run. In this case, the drift induced by switching gases is negligible compared to the drift induced by temperature, and is much less noticeable than the run at room temperature.

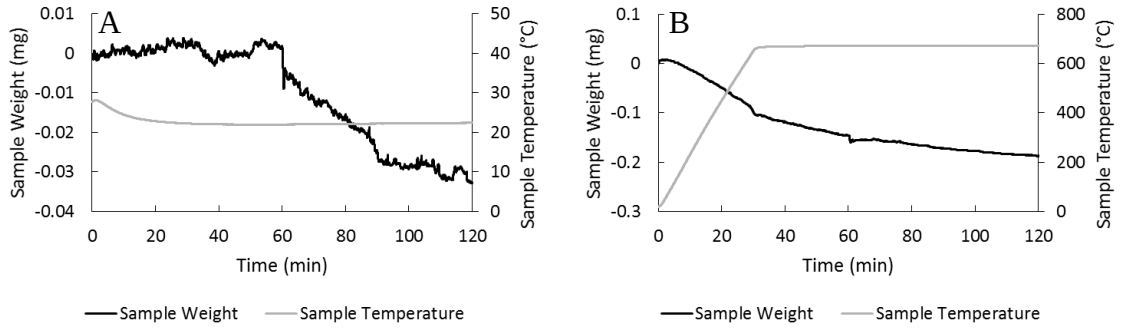

Figure 1. Weight trends and temperature trends of blank alumina pans at room temperature (A) and 670°C (B) versus reaction time. The first 60 minutes are under 200 mL/min of argon, and the time after that is under 200 mL/min of CO_2.

Beta zeolites were then run in the TGA to ensure instrument functionality. Zeolites are hygroscopic, and as such, will readily adsorb water from air. The adsorption capacity of H-Beta zeolite for water can be 10-15% weight percent at ambient conditions, depending on the

silicon/aluminum ratio of the sample. Thus, Beta zeolite samples should lose water weight upon heating. **Figure 2** depicts the weight loss of these zeolites as they were heated up to 600°C and 650°C under argon at a rate of 20°C/min, and the samples behaved as expected. At 600°C, the zeolite sample lost 11.9% of its weight, and at 650°C, the zeolite sample lost 11.7% of its weight. Both values agree with results reported in the literature, in which zeolite samples lost about 12% of their weight when heated in a TGA (Perraki and Orfanoudaki 2004).

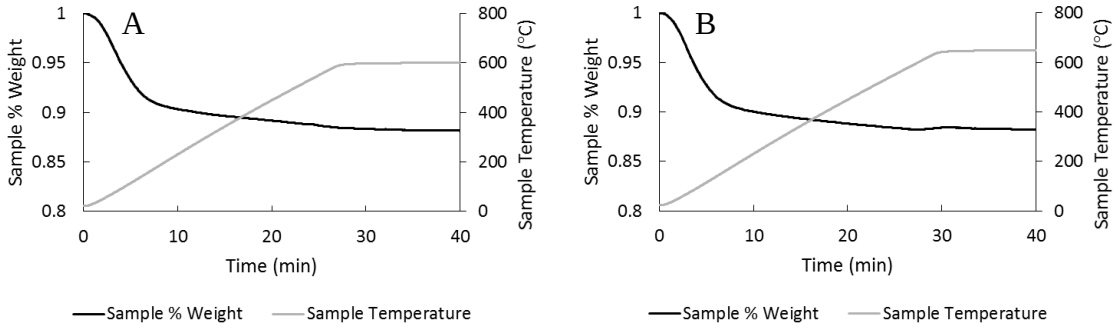

Figure 2. Weight trends and temperature trends of beta zeolites at 600°C (A) and 650°C (B) versus reaction time at a ramp rate of 20°C/min under 200 mL/min of argon.

To further validate TGA function, calcium acetate was decomposed at 750°C, at a ramp rate of 5°C/min. At a high enough temperature, calcium acetate will first lose a stoichiometric amount of water, and then should decompose into calcium carbonate and finally calcium oxide. As this was run at 750°C, there is no danger of forming unwanted $Ca(OH)_2$, as $CaCO_3$ begins to be favored at temperatures past 500°C. **Figure 3** depicts the aforementioned reactions of calcium acetate, and it is clear when and at which temperature the two distinct decompositions occur. The calcium acetate sample lost 8% in water weight, an additional 34% as it converted to calcium carbonate starting at about 400°C, and finally lost another 25% of its weight as it converted from calcium carbonate to calcium oxide, at about 600°C. The temperature at which these

decompositions occurred and the weight losses associated with the reactions agree quite well with values reported in the literature (Silaban, Narcida et al. 1992).

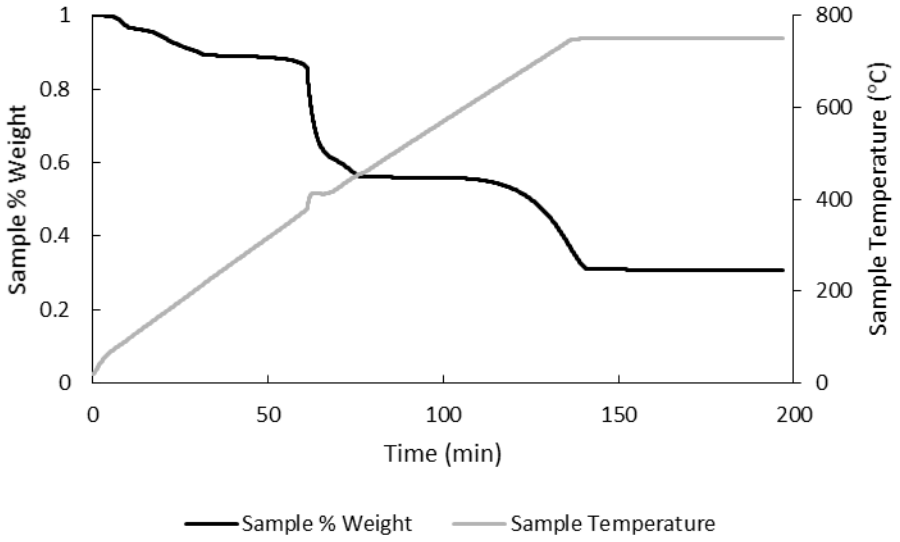

Figure 3. Weight trend and temperature trend of untreated calcium acetate versus reaction time, decomposed at 750°C at a ramp rate of 5°C/min under 200 mL/min of argon.

Results and Discussion: Calcium Oxide from Marble Study

Calcium oxide derived from marble was run in the TGA multiple times at the same reaction temperature of 650°C. For each of these runs, the gas flow rates of argon and CO_2, mesh size of particles, and pretreatment conditions were all constant, as was outlined in the Experimental section above. For all CaO-Marble samples presented here, the marble was pretreated in an open air oven at 650°C for eight hours at a ramp rate of 5°C/min. For every run in this study, the CaO-Marble sample was heated to 650°C under 200 mL/min argon at a rate of 20°C/min, and then pure CO_2 was fed at a flow rate of 200 mL/min after the reaction temperature was reached and mass had stabilized. The sample was then carbonated for about an hour. The objective of this study was to determine if the vendor-supplied calcium oxide is heterogeneous. Furthermore, the effect of sample age since last pretreatment, and number of pretreatments were studied as well, to

examine if reaction rates or conversion trends were altered. **Figure 4** charts the conversion trends and reaction rates from a single sample of calcium oxide (Sample A) from marble, pretreated once. This single pretreatment is designated as PT1 in the figures. In terms of conversion, all of the presented runs behaved similarly. Taking a closer look at the reaction rates in the first five minutes of carbonation however, it looks as if the oldest sample, which was ran 13 days after its pretreatment, experienced a greater reaction rate compared to the other, younger samples.

The conversion after one hour of carbonation and the peak reaction rates of the different samples are also presented in **Figure 4**, to give a general idea of the range of values that arise within these experiments. After one hour of carbonation, conversion for these samples ranged from 15.3% to 18.9%, with no clear trend in conversion as a function of sample age. However, the peak reaction rates experienced a slight trend upwards as the sample aged, with the final run experiencing a large jump. The peak reaction rates for this sample of untreated and aged marble ranged from 0.067 to 0.096 mols of CO_2 per minute. These variabilities in conversion and reaction rate for a single sample are only due to the sample age, and should be kept in consideration for future experiments.

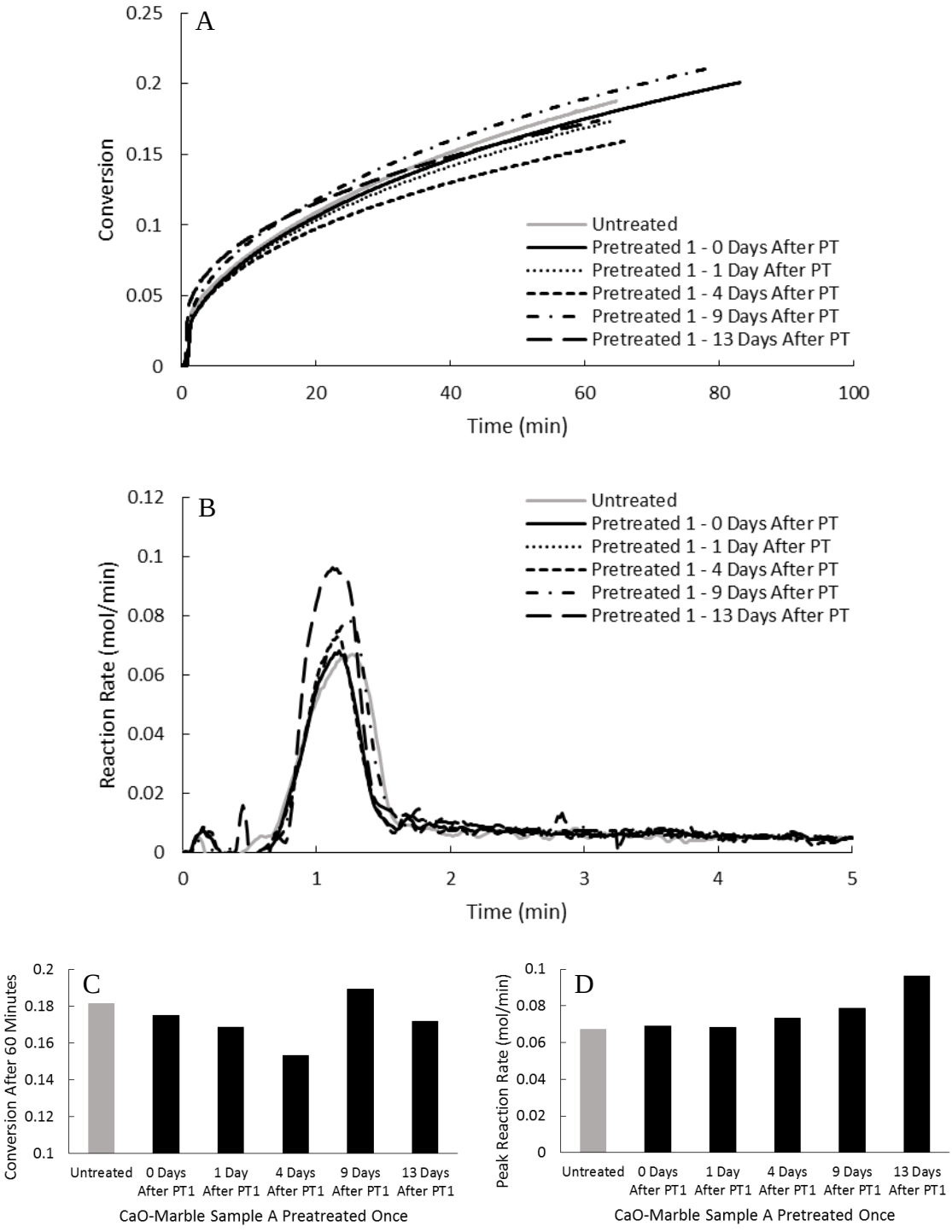

Figure 4. Conversion trend (A) and reaction rate (B) of CaO-Marble Sample A carbonation versus reaction time under 200 mL/min of 100% CO_2 at 650°C. Conversion after 60 minutes of carbonation (C) and peak reaction rates (D) are also presented. The pretreated samples were pretreated once at 650°C in an open air oven for 8 hours at a ramp rate of 5°C/min. The different lines and bars represent data for experiments that were run on an untreated sample and on pretreated samples after various days after their pretreatment.

This CaO-Marble Sample A was then pretreated again after 14 days in an open air oven at 650°C for eight hours at a ramp rate of 5°C/min, creating PT2, to explore the possible effects of multiple pretreatments on conversion and reaction rate. Calcium oxide is hygroscopic and is known to pick up water and CO_2 from laboratory air at ambient conditions (Morales-Flórez, Santos et al. 2015). The calcium oxide samples are kept in simple glass and plastic vials and tubes, and may pick up unwanted constituents in-between experiments. Because of this, multiple pretreatments may be utilized to ensure reproducibility. **Figure 5** below compares the conversion trends and reaction rates between Sample A calcium oxide runs that were pretreated once and the calcium oxide runs that were pretreated twice. In these experiments, the sample was heated to reaction temperature under 200 mL/min of argon, before 100% CO_2 was fed into the TGA at 200 mL/min to induce carbonation. While conversion trends seemed similar between these runs, it can be seen that the reaction rate of the older sample was greater than the younger samples, just as was seen earlier. **Figure 5** also shows the conversion after one hour of carbonation, and the peak reaction rates. The conversion after one hour of carbonation experienced a tighter spread of values with no significant deviation from expectation, ranging from 16.5% to 18.2%. The peak reaction rates ranged between 0.064 to 0.085 mols of CO_2 per minute, which is a little tighter than the sample that was pretreated once only.

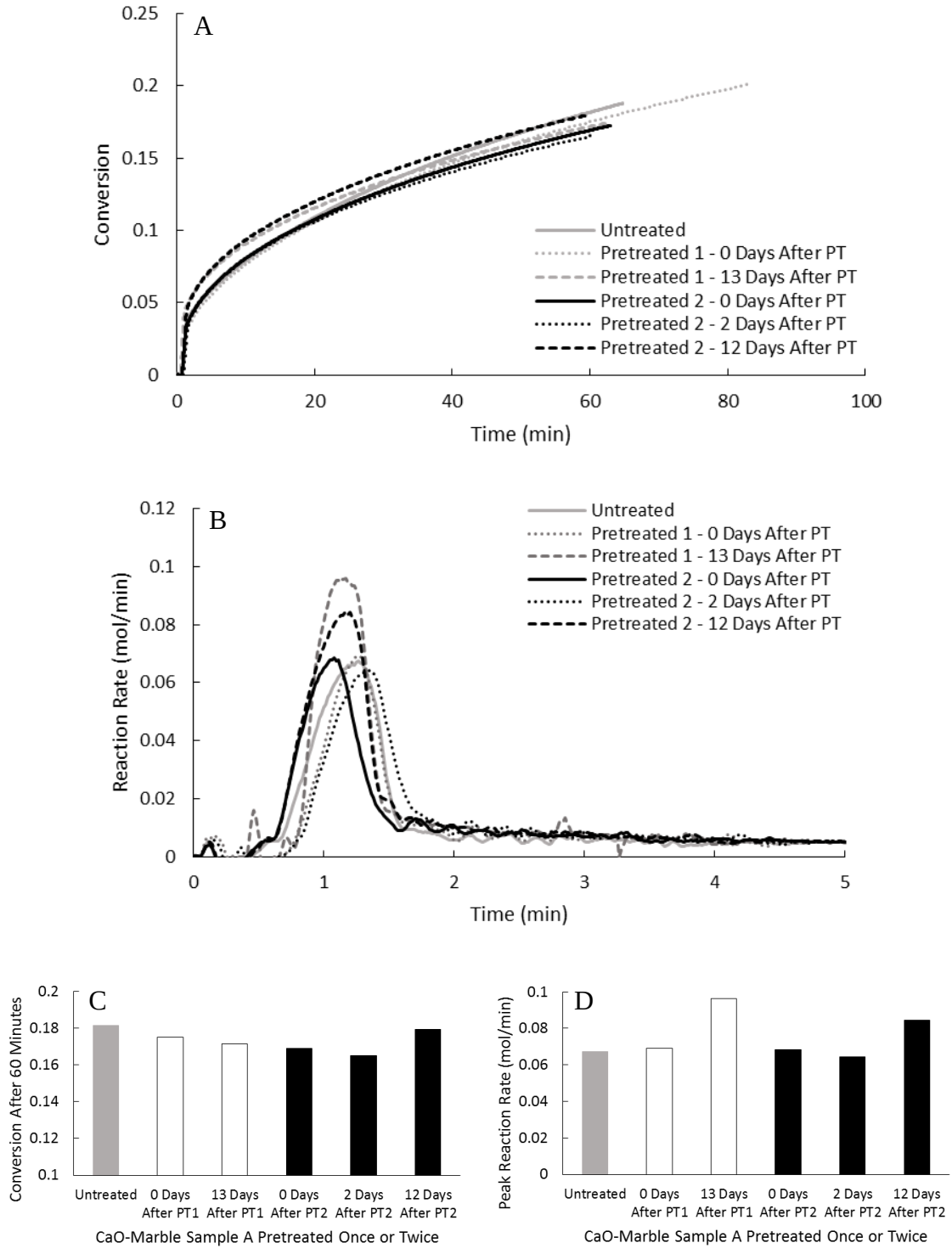

Figure 5. Conversion trend (A) and reaction rate (B) of CaO-Marble Sample A carbonation versus reaction time under 200 mL/min of 100% CO_2 at 650°C. Conversion after 60 minutes of carbonation (C) and peak reaction rates (D) are also presented. The pretreated samples were pretreated at 650°C in an open air oven for 8 hours at a ramp rate of 5°C/min 14 days after their first pretreatment. The different lines and bars represent data for experiments that were run on an untreated sample and on pretreated samples after various days after their second pretreatment. Samples pretreated once (grey lines and white bars) are shown for comparison.

This phenomenon of calcium oxide picking up moisture, CO_2, or other impurities from the air can be seen from the plots in **Figure 6**, in which the mass profiles of the calcium oxide samples under 200 mL/min of argon at a temperature ramp rate of 20°C/min and before carbonation are shown. With the exception of the 4 day old sample, as the sample ages, it experiences larger mass gains under argon, which can be explained by impurities in the sample reacting with impurities in the gaseous phase. The 9 day and 13 day old sample also stabilized to a mass lower than the other runs, which may indicate that these two samples had more time to age and pick up impurities after it was freshly pretreated. **Figure 7** depicts the mass trends under argon of the samples that were pretreated twice, in which the same phenomenon is observed. With a few exceptions, the general trend is that as the sample ages, it experiences larger mass gains, and stabilizes at a lower mass temperature, implying it may have picked up more constituents than the other untreated or fresher samples.

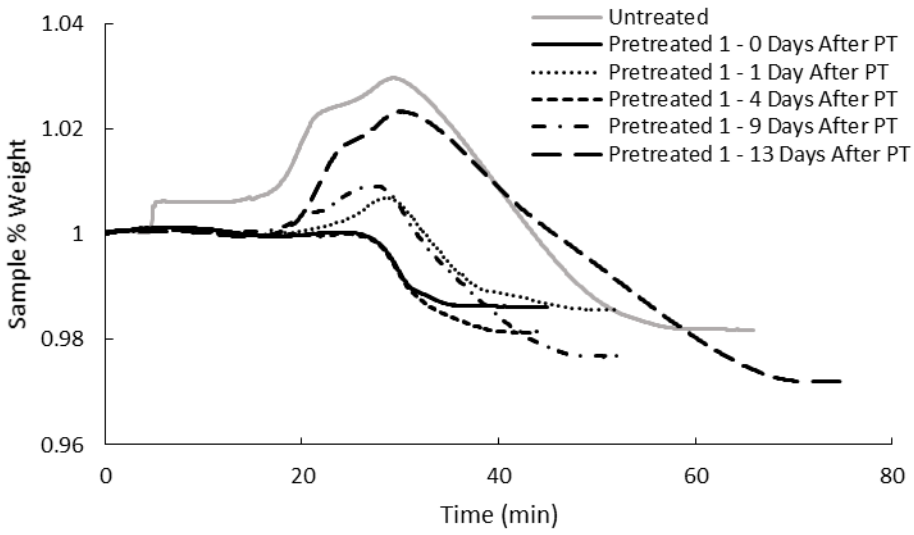

Figure 6. Weight trend of CaO-Marble Sample A versus reaction time under 200 mL/min of argon at 650°C. The pretreated samples were pretreated once at 650°C in an open air oven for 8 hours at a ramp rate of 5°C/min. The different lines represent data for experiments that were run on an untreated sample and on pretreated samples after various days after their pretreatment.

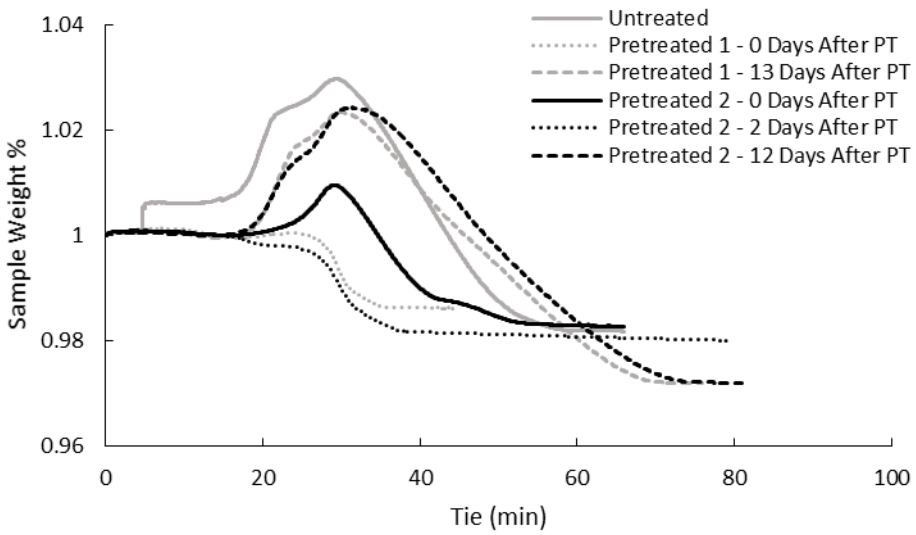

Figure 7. Weight trend of CaO-Marble Sample A versus reaction time under 200 mL/min of argon at 650°C. The samples pretreated twice were pretreated at 650°C in an open air oven for 8 hours at a ramp rate of 5°C/min 14 days after their first pretreatment. The different lines represent data for experiments that were run on an untreated sample and on pretreated samples after various days after their second pretreatment. Samples pretreated once (grey lines) are shown for comparison.

Now that the relative magnitudes of the effects of sample age and number of pretreatments on carbonation conversion and reaction rates has been established, the next step was to determine the behavior of a different sample of CaO-Marble. A new sample taken straight from the vendor-supplied bottle, named Sample B, was crushed, sieved, and pretreated in an open air oven at 650°C for eight hours at a ramp rate of 5°C/min, the same exact conditions as Sample A. In **Figure 8** below, it seems that the untreated sample did not experience a large mass gain under argon. However, after pretreating the sample and waiting two weeks, a large mass gain can be seen. Perhaps for some samples of calcium oxide, the pretreatment is necessary to allow for the picking up of constituents from the atmosphere. No matter what chemical or physical phenomena is causing this behavior, it is clear that the vendor-supplied calcium oxide is extremely varied and heterogeneous.

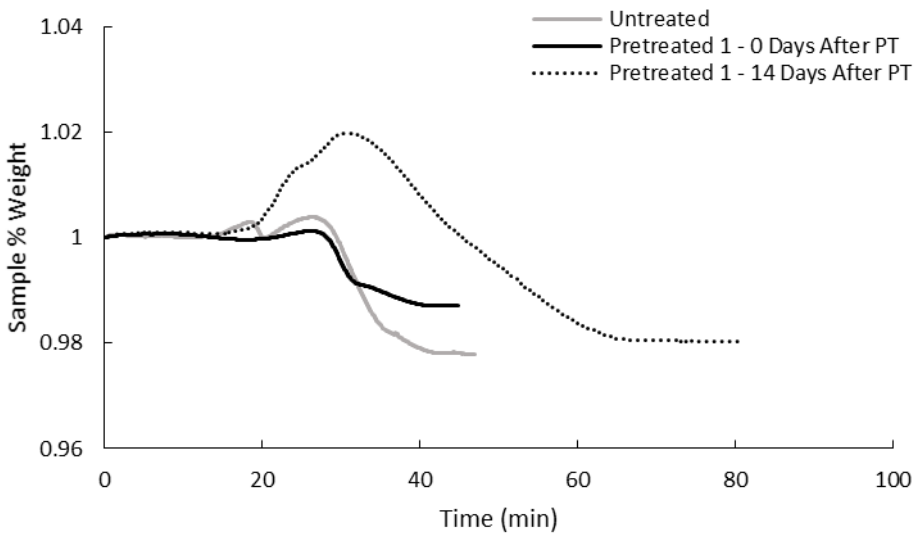

Figure 8. Weight trend of CaO-Marble Sample B versus reaction time under 200 mL/min of argon at 650°C. This new sample B was pretreated at 650°C in an open air oven for 8 hours at a ramp rate of 5°C/min. The different lines represent data for experiments that were run on an untreated sample B and on pretreated samples immediately and 14 days after their pretreatment.

This CaO-Marble Sample B was then carbonated and its conversion and reaction rate data were compared to Sample A, in which their trends are shown in **Figure 9**. It can be seen that generally, the Sample B runs performed closer to each other than the graphed Untreated A plot, provided for reference. However, the reaction rate trends seemed to be in-line between the two samples, with no large deviations. **Figure 9** also plots the conversion of the Sample B runs after one hour of carbonation, and their peak reaction rates. The Sample B conversion ranged from 11.6% to 14.3%, which is not within the range of the Sample A runs presented earlier. However, Sample B peak reaction rates fell well within the ranges presented earlier. The trend of increasing peak reaction rate as a function of time is observed in this sample as well.

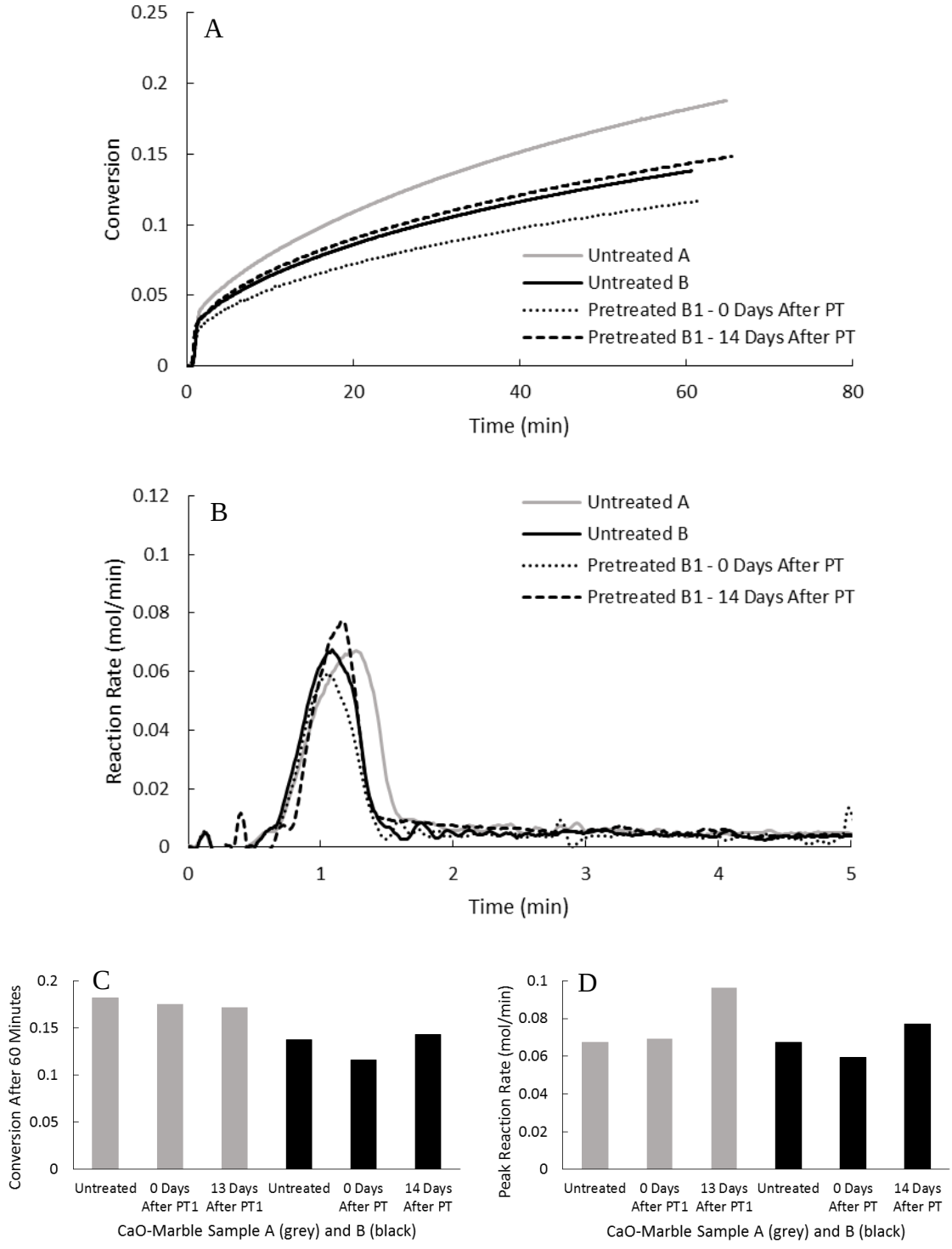

Figure 9. Conversion trend (A) and reaction rate (B) of CaO-Marble Sample B carbonation versus reaction time under 200 mL/min of 100% CO_2 at 650°C. Conversion after 60 minutes of carbonation (C) and peak reaction rates (D) are also presented. The pretreated samples were pretreated once at 650°C in an open air oven for 8 hours at a ramp rate of 5°C/min. The different lines and bars represent data for experiments that were run on an untreated sample B and on pretreated samples immediately and 14 days after their pretreatment. CaO-Marble Sample A data (grey lines and bars) are shown for comparison.

Conversion and reaction rate trends for both Sample A and Sample B runs were then compared to a new sample of CaO-Marble. This new Sample C was pretreated at 650°C for eight hours at a ramp rate of 5°C/min, and then carbonated in the TGA. Its comparison to Sample A and Sample B at a reaction temperature of 650°C are shown below in **Figure 10**. All three samples were freshly pretreated before carbonation, and the magnitude of ranges for intra-sample variances given earlier do not explain the observed discrepancy with Sample C. It is quite obvious that Sample C's reaction rate trend and peak reaction rates will vary greatly from Sample A and B, as it experiences a much larger carbonation.

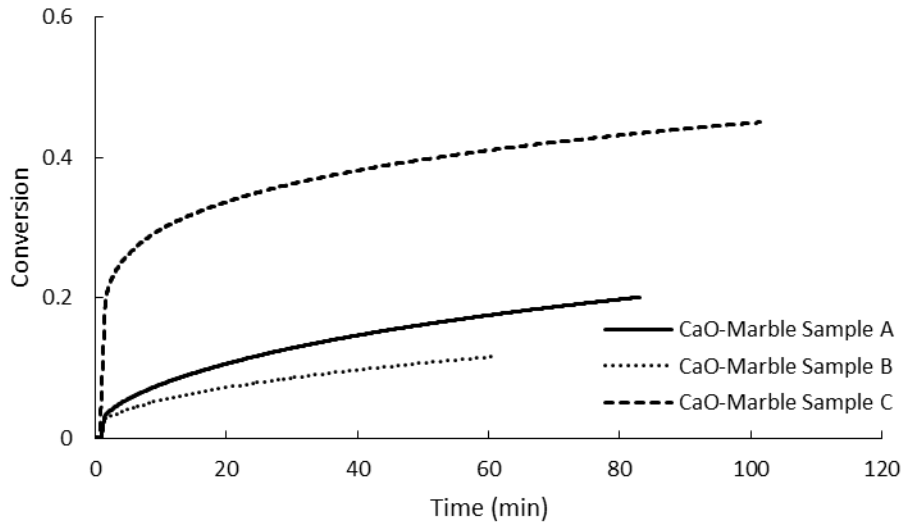

Figure 10. Conversion trend of CaO-Marble Samples A, B, and C versus reaction time under 200 mL/min of 100% CO_2 at 650°C.

With this study of various CaO-Marble samples, it can be seen that the vendor supplied vial contains product that is wildly heterogeneous. From Sample A, multiple pretreatments seem to not affect conversion nor reaction rates significantly. There is no strong trend in conversion as the sample ages. However, there is a slight effect of sample age on the peak reaction rate, as it

trends upwards as the sample ages from its last pretreatment. This slight effect should be kept in mind as further analysis of the carbonation of these calcium oxide samples is pursued. With that being said, Sample C will be utilized for the following experiments, in which the effect of temperature on carbonation is studied. Sample C will also be compared to other calcium oxide samples derived from calcium acetate and nanofibers.

Results and Discussion: Calcium Oxide Various Precursors Study

CaO-Marble Sample C (referred to as CaO-Marble from now on) was carbonated at different temperatures, to test the effect of temperature on the carbonation kinetics of the system. With gas flow rates, CO_2 partial pressure, software commands, and initial sample size kept constant, reaction temperature was swept from 600°C to 800°C in 50°C increments. In each run, the sample is heated to reaction temperature under 200 mL/min of argon at a ramp rate of 20°C/min until mass and temperature stabilizes. At this point, the fed gas switches to pure CO_2 at 200 mL/min, and the sample is carbonated for about an hour. The conversion trends and reaction rates for these five runs are presented below in **Figure 11**. Generally, as temperature increases, conversion increases as well. This is a well-known phenomenon and is demonstrated in other papers as well (Zhou, Xu et al. 2013). However, interestingly enough, there is no clear increase in peak reaction rates as a function of temperature, as can be seen by the given reaction rate trends. This indicates that at higher temperatures, the sample is undergoing carbonation for a longer time. The reaction rate trend does not increase vertically with temperature, but horizontally. The area under the curve of the reaction rate trends increases with temperature, causing a larger overall conversion.

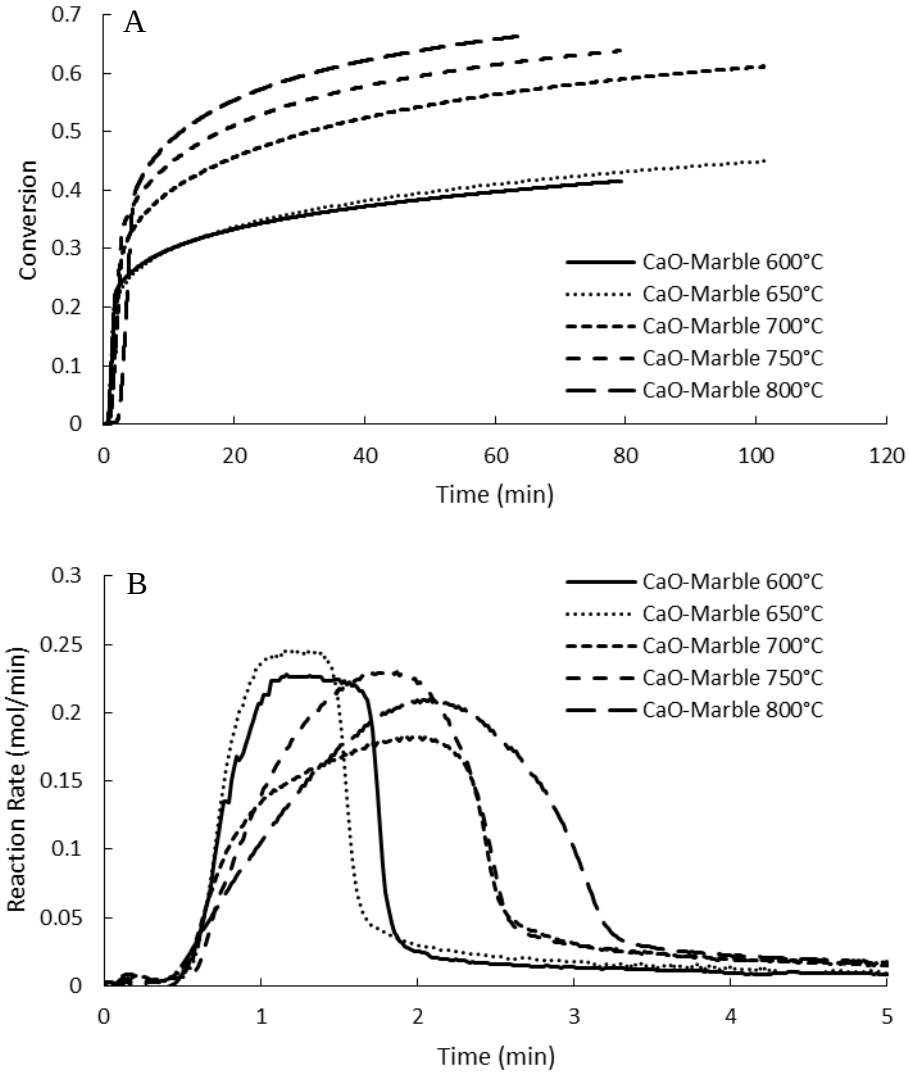

Figure 11. CaO-Marble conversion trend (A) and reaction rates (B) versus reaction time at various temperatures. The CaO-Marble was pretreated in an open air oven at 650°C for 8 hours at a ramp rate of 5°C/min. In each run, the CaO-Marble was heated up to reaction temperature under 200 mL/min of argon. The sorbent was then carbonated under 200 mL/min of 100% CO_2. The different lines represent data for experiments that were run at various reaction temperatures, ranging from 600°C to 800°C.

The same experiments were run on a CaO-CaAcetate sample. **Figure 12** depicts the conversion and reaction rate trends of these samples, which ran from 600°C to 800°C. Again, there is no clear or obvious trend in their peak reaction rates, just as was observed with the CaO-Marble samples from earlier. However, there is a clear effect of temperature on conversion, as samples carbonated under higher temperatures reached much higher conversions. The sample carbonated

at 800°C was even seemingly completely converted into $CaCO_3$. It should be noted that the values of both conversions and reaction rates are significantly greater than what was experienced with CaO-Marble samples. This indicates that although both samples are calcium oxide, there is some inherent differences between the materials that come about as a function of what precursor material the calcium oxide was derived from, as mentioned earlier. In this case, much like the CaO-Marble samples, the large reaction rate stays for a longer time at higher temperatures. However, the effect is much less pronounced in the CaO-CaAcetate sample, which is evident in the conversion trends, in which temperature had a smaller effect on conversion, compared to the CaO-Marble sorbent.

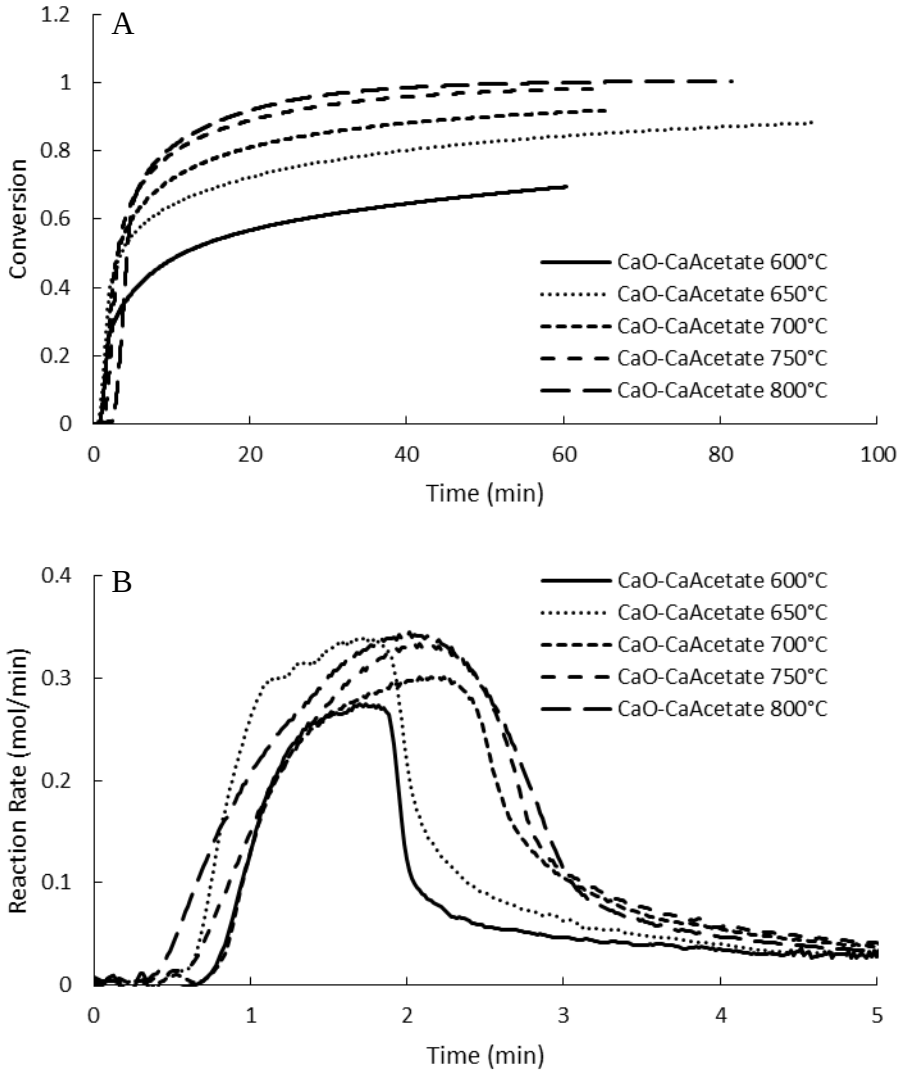

Figure 12. CaO-CaAcetate conversion trend (A) and reaction rates (B) versus reaction time at various temperatures. The CaO-CaAcetate was prepared by heating in an open air oven at 750°C for 8 hours at a ramp rate of 5°C/min. In each run, the CaO-CaAcetate was heated up to reaction temperature under 200 mL/min of argon. The sorbent was then carbonated under 200 mL/min of 100% CO_2. The different lines represent data for experiments that were run at various reaction temperatures, ranging from 600°C to 800°C.

Like the CaO-Marble and CaO-CaAcetate samples presented earlier, CaO-NF samples were ran in the TGA at a range of temperatures from 600°C to 800°C. The conversion trends and reaction rates can be seen in **Figure 13**. At first glance, it is apparent that compared to the CaO-Marble and CaO-CaAcetate sorbents, the CaO-NF sorbent experienced a much higher conversion at an earlier time and at a lower temperature. The peak reaction rates again seem to not show a

strong dependence with temperature. In the CaO-NF case, the temperature dependence of conversion is much less obvious because even at low temperatures, the upper limit of 100% is being reached easily. It seems that at any temperature above 650°C, the sample will carbonate completely and reach full conversion. Similar to the behavior of the CaO-Marble and CaO-CaAcetate sorbents, increasing temperature seems to not increase the peak reaction rates, but does have an effect on the length of time the sorbent is within the kinetically controlled region. This higher temperature seems to elongate the time of the fast carbonation period, potentially providing the required energy to push the sorbent and gaseous phase together to react for a longer time, before the system finally switches to a more diffusion controlled region.

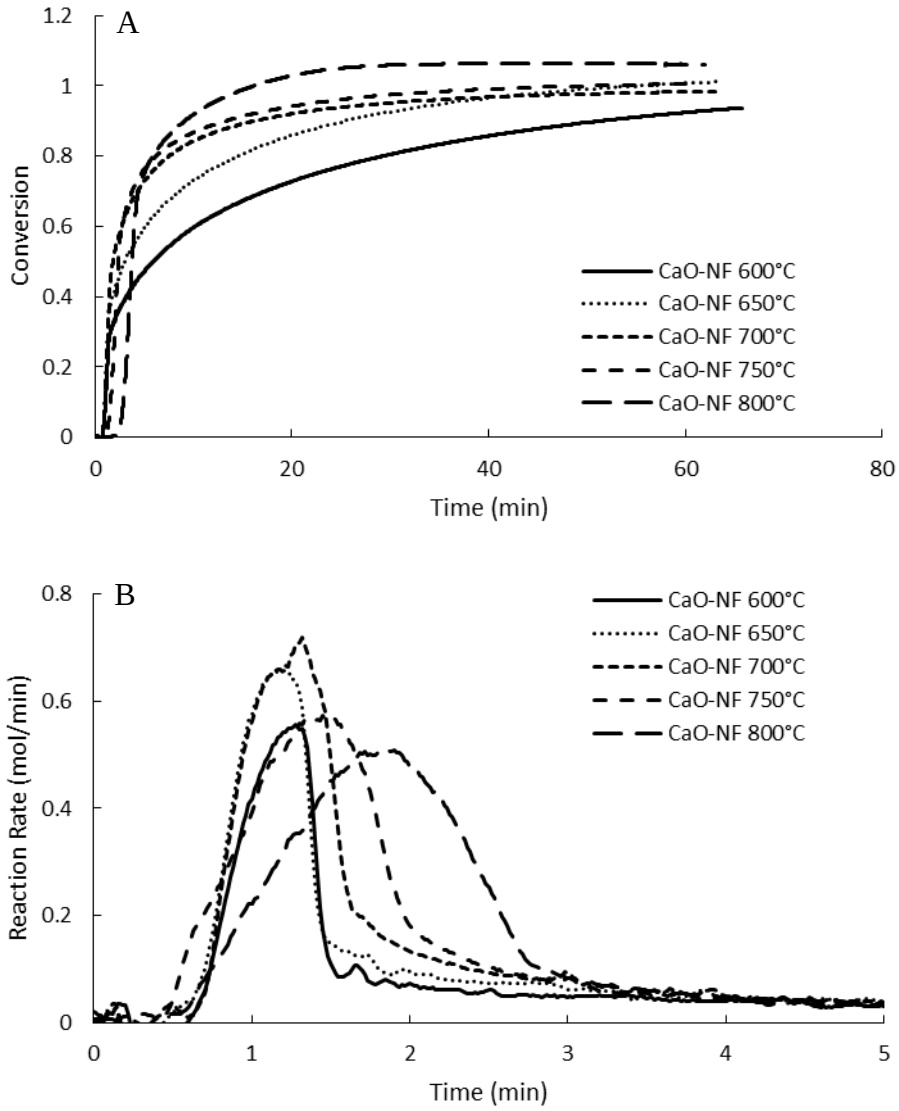

Figure 13. CaO-NF conversion trend (A) and reaction rates (B) versus reaction time at various temperatures. The CaO-NF was prepared in an electrospinning chamber, and then pretreated in an open air oven at 500°C and 650°C for 8 hours at a ramp rate of 5°C/min. In each run, the CaO-NF was heated up to reaction temperature under 200 mL/min of argon. The sorbent was then carbonated under 200 mL/min of 100% CO_2. The different lines represent data for experiments that were run at various reaction temperatures, ranging from 600°C to 800°C.

However, an interesting phenomenon is observed at 800°C. The sample reached a weight that indicated a conversion greater than 100%, reaching 106% conversion. To eliminate the possibility of a taring or experimental issue, the CaO-NF sorbent was carbonated at 800°C two

additional times. The trends for these runs are plotted in **Figure 14** below, and it can be seen that the conversion behaves similarly between all three runs.

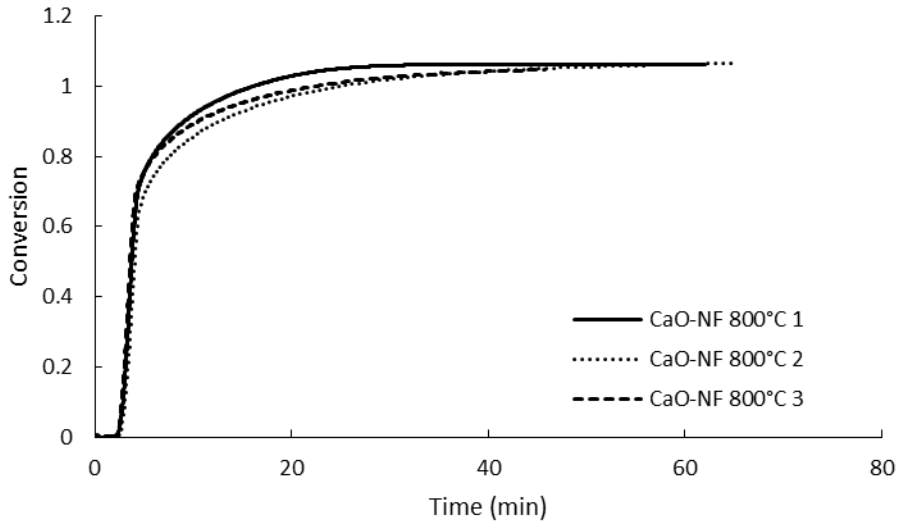

Figure 14. CaO-NF conversion trend versus reaction time. The CaO-NF was prepared in an electrospinning chamber, and then pretreated in an open air oven at 500°C and 650°C for 8 hours at a ramp rate of 5°C/min. The different lines represent data for three replicate experiments. In each run, the CaO-NF was heated up to reaction temperature under 200 mL/min of argon. The sorbent was then carbonated under 200 mL/min of 100% CO_2.

In all of the replicate runs, they very quickly reached and surpassed 100% conversion in about twenty minutes. According to the earlier experiments that determined possible TGA drift, the sample was capable of drifting 0.2 mg at 650°C. Assuming a worst case scenario of 0.2 mg drift, the extra conversion past 100% can be explained by instrument error. This drift is also exacerbated by the fact that the bulk density of the CaO-NF sorbent is so low that only 3-4 mg of sample can fit in the pan, which increases the ratio of the magnitude of the drift to the magnitude of the experimental data. Thus, this 0.2 mg drift plays a much larger role in the CaO-NF data than the CaO-Marble data, in which the original sample weight was around 16 mg. However from the conversion trends in **Figure 13**, the runs from 650°C to 750°C all reached about 100% conversion and stayed there for a long period of time. This may provide evidence that there is some underlying

mechanism that is being triggered at 800°C. Perhaps the physical properties of the sorbent at a molecular level have been altered such that the sorbent does not fully calcine at 800°C, but is still able to carbonate to complete conversion. Perhaps the high temperature is inducing an additional reaction with the gaseous CO_2, creating a new, unknown product. The high temperature may also be inducing some sort of physical melting or other alteration of the material. Further chemical testing of the sample before and after carbonation will provide more information as to whether this is an instrument issue, or an actual physical phenomena. Despite these anomalies, it is very clearly seen that the CaO-NF behaves much differently than CaO-Marble and CaO-CaAcetate under the same exact run conditions. This increased performance reinforces the initial hypothesis that the precursor of the calcium oxide plays a large part in determining its physical and chemical properties, which in turn, greatly affects sorbent activity.

It is clear from the conversion trends that CaO-NF activity is much greater than CaO-Marble and CaO-CaAcetate. The electrospun sorbent carbonated to a higher degree than the other two precursors, at all temperatures tested. The comparisons of the conversion trends between the sorbents are plotted in **Figure 15**, at 600°C and 800°C. The peak reaction rates for every run can also be plotted for comparison. From this graph in **Figure 15**, it is clear that CaO-NF experienced a much higher peak reaction rate across the temperatures that were swept, explaining its higher conversion. The CaO-Marble sorbents did not come close to complete conversion, as even at 800°C, the sample only reached about 65% conversion. The CaO-CaAcetate sorbent did reach complete conversion at 800°C, while the CaO-NF samples easily reached complete conversion at 650°C and above. Because of this much higher performance, perhaps the use of a nanofiber sorbent can potentially outweigh the low cost advantage of marble for use in an SE-SMR process.

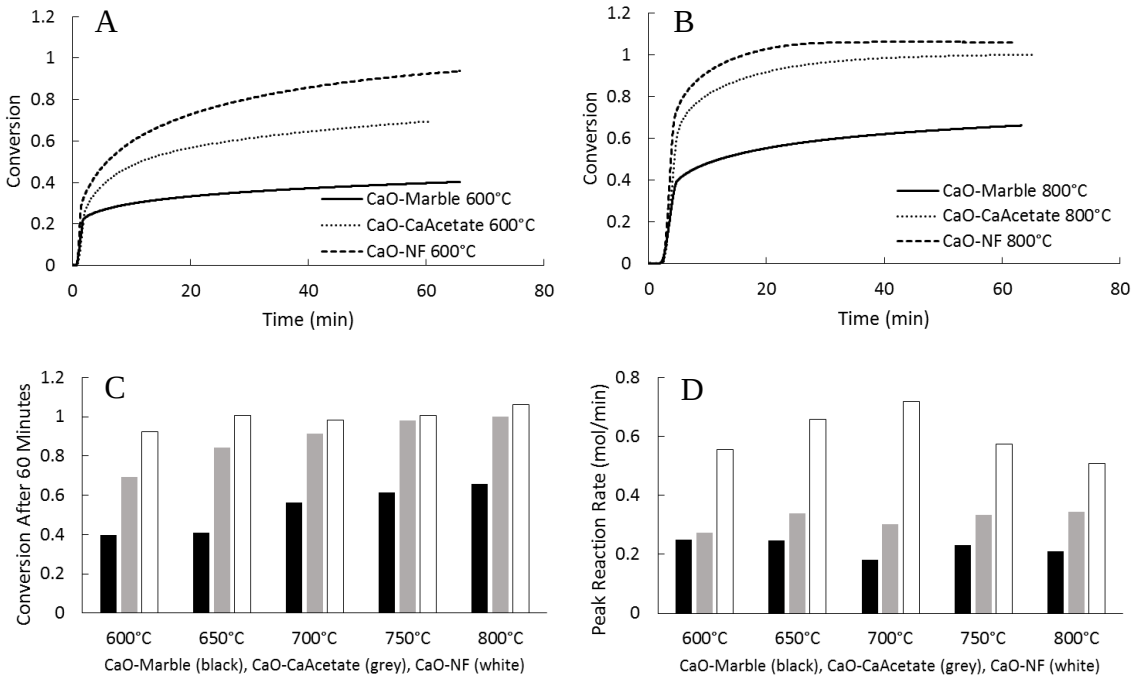

Figure 15. Conversion trends for three calcium oxide precursors at 600°C (A) and 800°C (B). Conversion after 60 minutes of carbonation (C) and peak reaction rates (D) are also shown, at a range of temperatures. CaO-Marble was pretreated in an open air oven at 650°C for 8 hours at a ramp rate of 5°C/min. CaO-CaAcetate was prepared by heating in an open air oven at 750°C for 8 hours at a ramp rate of 5°C/min. CaO-NF was prepared in an electrospinning chamber, and then pretreated in an open air oven at 500°C and 650°C for 8 hours at a ramp rate of 5°C/min. In each run, the sorbent was heated up to reaction temperature under 200 mL/min of argon. The sorbent was then carbonated under 200 mL/min of 100% CO_2 for about an hour.

Electrospun nanofibers have been known to sport a much higher surface area to volume ratio. Because calcium oxide carbonation is a surface reaction characterized by an abrupt shift between kinetically and diffusional controlled reactions, it makes sense as to why the CaO-NF sample performed much better than the other sorbents. When the carbonation first begins, the CO_2 diffuses from the bulk fluid onto the reactive surface of the sorbent. Because the experiment was designed such that the particle sizes were small and the gaseous phase flow rates were large, this external mass transfer is assumed to be negligible. Once the CO_2 reaches the reactive surface, the surface is immediately converted into $CaCO_3$ product. It is clear from the peak reaction rates that

the CaO-NF sorbent had many more easily reachable reactive sites, allowing the rapid creation of the product layer. As the diffusion of the CO_2 becomes the limiting factor in the reaction, the system transitions from the chemically controlled to the diffusion controlled region. Because the CO_2 requires time to diffuse through the newly formed $CaCO_3$ product layer, the higher porosity of the CaO-NF sorbent provides many opportunities for the CO_2 to travel through the relatively thinner product layers and reach the reactive sorbent. These factors serve to explain why CaO-NF seemingly outperforms the other two precursors during both regimes of carbonation.

Modeling Results and Discussion

Modeling Results and Discussion: Random Pore Model

Once **Equation 20** and **Equation 21** have been inputted into Athena along with the appropriate temperature and structural parameters, the conversion data taken from the TGA is then modified by implementing the correct Ψ value. This modified conversion data is then compared to the predicted results computed by the software using an initial guess for the three estimated parameters: k_{RPM}, D_{RPM}, and the switch time from the kinetically controlled region to the diffusion controlled region. The squared sum of the residual discrepancy between the modeled results and the observed data is calculated, and the software modifies its guesses for the three parameters such that this value is minimized. **Figure 16** depicts several example plots generated by Athena, comparing the observed modified conversion to the optimal predicted modified conversion for the CaO-Marble sample run at 600°C, 700°C, and 800°C. **Figure 17** depicts the generated plots from the parameter estimation process for the three precursors at 650°C. Note that the odd conversion trends are not the experimentally observed conversion, but is a modified conversion, which is a function of the sorbent's structural properties. This is why the conversions seem to surpass unity,

and why CaO-CaAcetate seems to perform better than CaO-NF. In addition to these plots, the three estimated parameters are also quantified.

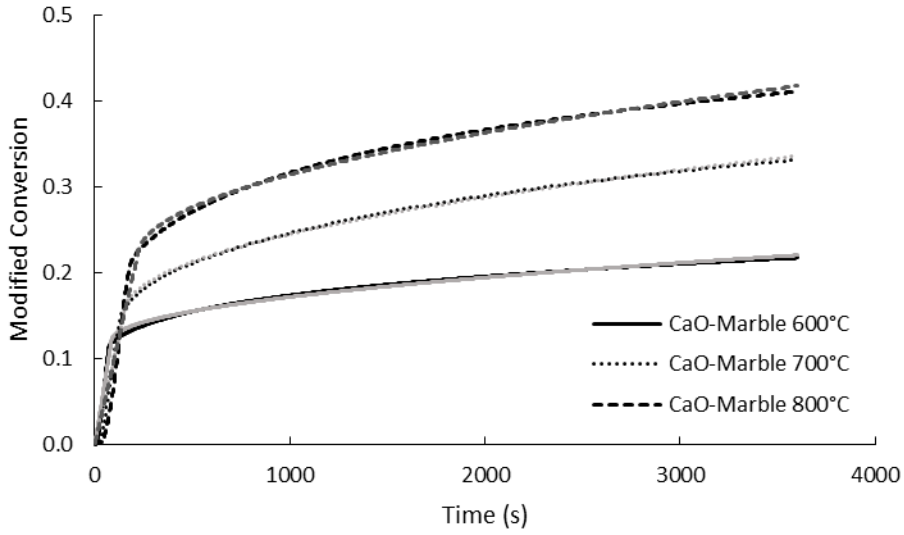

Figure 16. Athena parameter estimation output for the RPM, plotting modified conversion versus reaction time. Black data trends are from experiments, in which CaO-Marble was carbonated under 200 mL/min of 100% CO_2 at 600°C, 700°C, and 800°C. Grey data trends are model calculated values.

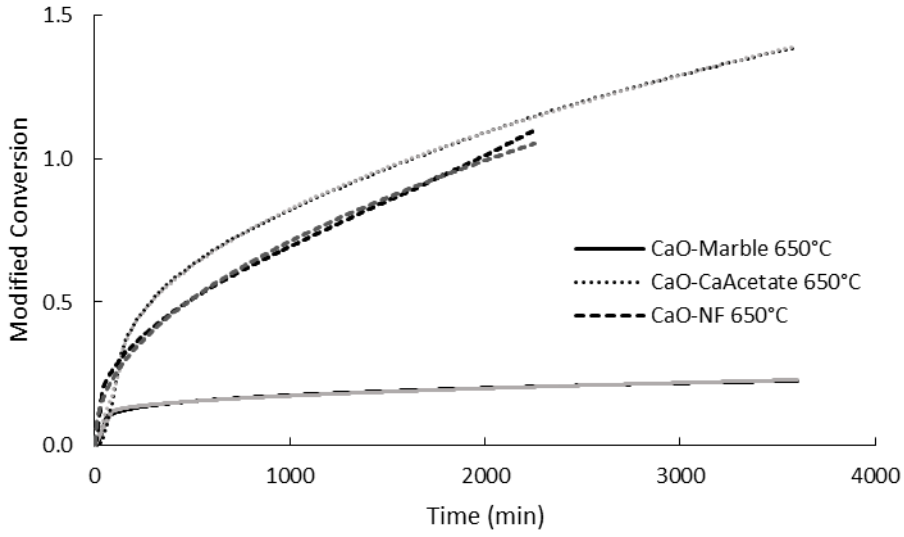

Figure 17. Athena parameter estimation output for the RPM, plotting modified conversion versus reaction time. Black data trends are from experiments, in which CaO-Marble, CaO-CaAcetate, and CaO-NF was carbonated under 200 mL/min of 100% CO_2 at 650°C. Grey data trends are model calculated values.

This analysis was then repeated for all three precursors, at all of the different temperatures in which they were tested at. It should be noted that the conversion data from the TGA was transformed to the modified conversion, as per **Equation 20** and **Equation 21**. Because of this, the modified conversion deviates from the intended trend at conversion values very close to unity, and is undefined at conversions beyond it due to the natural logarithmic nature of the equation. For this reason, the data was trimmed to remove any value past unity, or any value that seemed to cause the modified conversion to deviate from a square root of time dependence. This trimming was only necessary for the high performance runs, including the CaO-CaAcetate run at 800°C, and a few CaO-NF runs as well. The results are summarized in **Table 3**, and visualized in **Figure 18**. It is clear that CaO-Marble severely underperforms compared to the other two sorbents, with CaO-CaAcetate sporting surprisingly high values.

Table 3. Summary of modeling results from the RPM. Athena's optimized k_{RPM} and D_{RPM} and their 95% confidence intervals are presented for CaO-Marble, CaO-CaAcetate, and CaO-NF at a range of temperatures. Optimized switch time and its interval is also presented.

Precursor	Temperature	k_{RPM} (m^4/mol/s)	D_{RPM} (m^2/s)	Switch Time (s)
Marble	600°C	$2.6 \times 10^{-12} \pm 1.8 \times 10^{-14}$	$8.4 \times 10^{-18} \pm 5.9 \times 10^{-20}$	86 ± 1
	650°C	$2.6 \times 10^{-12} \pm 2.2 \times 10^{-14}$	$12 \times 10^{-18} \pm 8.1 \times 10^{-20}$	84 ± 1
	700°C	$2.1 \times 10^{-12} \pm 1.2 \times 10^{-14}$	$32 \times 10^{-18} \pm 20 \times 10^{-20}$	153 ± 1
	750°C	$2.4 \times 10^{-12} \pm 1.7 \times 10^{-14}$	$40 \times 10^{-18} \pm 37 \times 10^{-20}$	166 ± 2
	800°C	$2.3 \times 10^{-12} \pm 1.5 \times 10^{-14}$	$43 \times 10^{-18} \pm 50 \times 10^{-20}$	218 ± 2
Calcium Acetate	600°C	$3.5 \times 10^{-12} \pm 4.0 \times 10^{-14}$	$1.7 \times 10^{-16} \pm 1.4 \times 10^{-18}$	125 ± 2
	650°C	$5.4 \times 10^{-12} \pm 2.4 \times 10^{-14}$	$3.8 \times 10^{-16} \pm 1.6 \times 10^{-18}$	131 ± 1
	700°C	$5.1 \times 10^{-12} \pm 3.4 \times 10^{-14}$	$6.7 \times 10^{-16} \pm 4.5 \times 10^{-18}$	180 ± 2
	750°C	$5.7 \times 10^{-12} \pm 2.3 \times 10^{-14}$	$23 \times 10^{-16} \pm 5.4 \times 10^{-18}$	125 ± 1
	800°C	$4.8 \times 10^{-12} \pm 12 \times 10^{-14}$	$49 \times 10^{-16} \pm 3.6 \times 10^{-18}$	82 ± 2
Nanofibers	600°C	$3.9 \times 10^{-12} \pm 4.5 \times 10^{-13}$	$2.0 \times 10^{-16} \pm 8.0 \times 10^{-19}$	10 ± 1
	650°C	$5.7 \times 10^{-12} \pm 14 \times 10^{-13}$	$4.3 \times 10^{-16} \pm 34 \times 10^{-19}$	6 ± 2
	700°C	$4.1 \times 10^{-12} \pm 0.3 \times 10^{-13}$	$2.7 \times 10^{-16} \pm 14 \times 10^{-19}$	96 ± 1
	750°C	$3.8 \times 10^{-12} \pm 0.5 \times 10^{-13}$	$6.0 \times 10^{-16} \pm 45 \times 10^{-19}$	71 ± 1

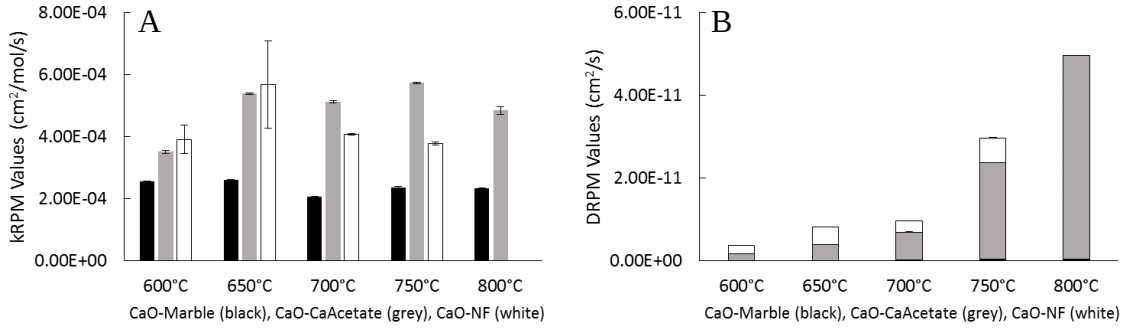

Figure 18. Athena parameter estimation output for the RPM, plotting optimized k_{RPM} (A) and D_{RPM} (B) values for CaO-Marble (black), CaO-CaAcetate (grey), and CaO-NF (white) at a range of temperatures.

The error bars of the parameters in **Figure 18** are the 95% confidence intervals that Athena calculates. These confidence intervals accounted for 95% of the potential deviance from the optimal parameter guesses, and are almost always about two orders of magnitude lower than the optimal parameter guess. This indicates that these estimated parameters can be interpreted confidently for the system, as each estimated parameter had a low coefficient of variance. The only exception is within the CaO-NF run at 650°C, as the software was not able to generate a confident value for the k_{RPM} nor the switch time. The R-square value is also calculated by Athena and is given for each analyzed run. An R-square value close to unity indicates that the model captures the data well, and is able to safely predict where the observed values will lie. From the confidence intervals in **Table 3**, and the R-square values and the sum of the squared residuals given in **Table 4**, it can be seen that the RPM faithfully captures the observed conversion trends, at least statistically. The CaO-Marble runs sport the lowest sum square of residuals, indicating that the model has a little bit of trouble capturing the more dramatic CaO-CaAcetate and CaO-NF trends. This is further supported by the fact that all three sorbents have a larger sum square of residuals as temperature increases, as the conversion increases and more prominent features of the conversion trends are exhibited.

Table 4. Athena's calculated R-squared values and sum of squared residuals for each RPM run, for each of the three precursors at a range of temperatures.

Precursor	Temperature	R^2 Value	Sum of Squared Residuals
Marble	600°C	0.99	0.02
	650°C	0.99	0.02
	700°C	1.00	0.05
	750°C	1.00	0.12
	800°C	0.99	0.18
Calcium Acetate	600°C	0.99	0.23
	650°C	1.00	0.17
	700°C	1.00	0.55
	750°C	1.00	0.21
	800°C	0.99	1.75
Nanofibers	600°C	1.00	0.40
	650°C	0.99	0.73
	700°C	1.00	1.10
	750°C	0.99	1.40

For the CaO-Marble, CaO-CaAcetate, and CaO-NF runs that were analyzed under the RPM, there does not seem to be a trend in the k_{RPM} values as temperature is increased. This is contrary to what previous work has shown in which the rate coefficients behaved in an Arrhenius fashion, allowing for the calculation of a pre-exponential factor and an activation energy for the kinetically controlled region (Grasa, Murillo et al. 2009, Zhou, Xu et al. 2013). However, the k_{RPM} values for the CaO-CaAcetate and CaO-NF samples are greater than their respective CaO-Marble counterparts. Interestingly enough, the CaO-NF did not sport significantly higher k_{RPM} than the CaO-CaAcetate despite reaching much higher conversions. However, it should be noted that the

structural parameters of the CaO-NF were roughly estimated from the marble sample that was used to create the sorbent, and may be inaccurate. This rate constant value should only be a function of the system parameters such as chemical constituents, concentrations, and temperature, and not the structural parameters of the sorbent being used. As such, this discrepancy between the precursors' k_{RPM} values indicate that there is some underlying factor affecting this estimated parameter, or perhaps is indicative of a possible inaccuracy within the model itself. The RPM may be lumping other parameters into this rate constant, such as surface reactions or even molecular diffusion. This k_{RPM} may also account for some structural differences present at the molecular or nano-crystalline level within the sorbent, convoluting its true chemical meaning.

On the other hand, the D_{RPM} values for the CaO-Marble and CaO-CaAcetate exhibit a temperature dependence. Similarly to the k_{RPM} values presented earlier, CaO-CaAcetate performed better during the diffusion controlled region compared to CaO-Marble at all temperatures. In contrast to this, the D_{RPM} values for CaO-NF did not experience a temperature dependence, and were only larger than the CaO-Marble values. By plotting the natural logarithm of the diffusivities that did have a temperature dependence versus the inverse of temperature, an Arrhenius relationship can be observed, which is what has been reported in the literature (Grasa, Murillo et al. 2009, Zhou, Xu et al. 2013).

From the Arrhenius plot of the diffusivities in **Figure 19**, a pre-exponential factor and an activation energy for the diffusion controlled region can be calculated. For CaO-Marble, the calculated pre exponential factor is 1.4 x 10^{-13} m^2/s, which disagrees with the reported pre exponential factor for Imeco limestone of 3.4 x 10^{-6} m^2/s (Grasa, Murillo et al. 2009). The activation energy for CaO-Marble of 70.6 kJ/mol also disagrees with the reported value of 163 kJ/mol (Grasa, Murillo et al. 2009). These large discrepancies in pre exponential factor and

activation energy for the diffusion controlled region may be due to the high concentration of CO_2 being used. The RPM may not be fully accurate at higher partial pressures of the gaseous phase reactant, as the literature experiments that the calculated values are being compared against were run at lower pressures of CO_2. The RPM has been shown to be able to accurately predict TGA conversion data using estimated parameters within a temperature range of 500°C-700°C, and a CO_2 partial pressure range of 5%-15% (Zhou, Xu et al. 2013). The experiments presented here are well outside of this range, and may be the cause of the large discrepancies in estimated parameters. The same calculations can be done for the CaO-CaAcetate sorbent, which found that the activation energy for this system is 132 kJ/mol, while the pre exponential factor is 1.13 x 10^{-8} m^2/s. Both values are larger than the CaO-Marble's respective parameters.

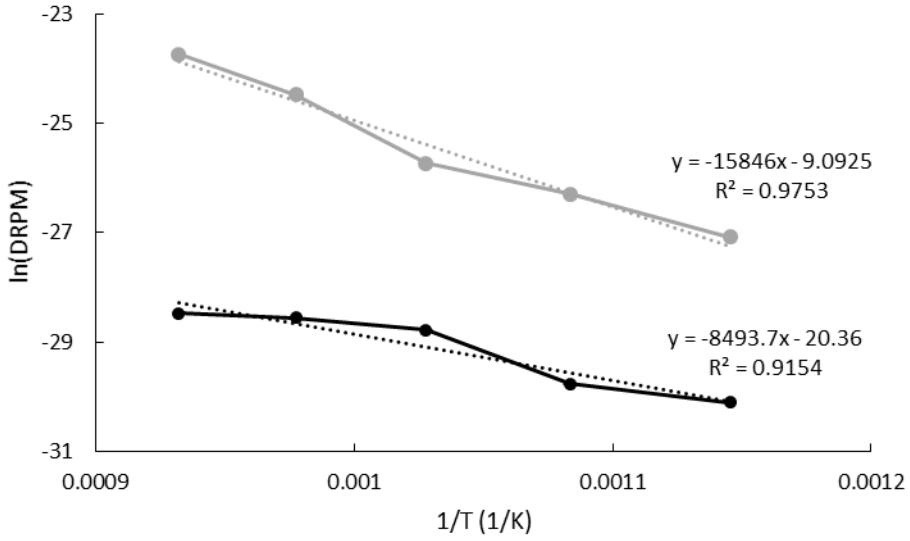

Figure 19. Arrhenius plot of D_{RPM} values for CaO-Marble (black) and CaO-CaAcetate (grey), calculated from Athena parameter estimation output for the RPM. The natural log of the D_{RPM} is plotted versus the inverse of the temperature in which that particular value was obtained at.

The fact that the k_{RPM} seemingly showed no temperature dependence, while the D_{RPM} did for some samples, may be indicative that the sorbent is being bombarded with the 100% partial

pressure of the CO_2 reactant, such that the kinetically controlled region is nonexistent. This is further supplemented by the peak reaction rates presented in **Figure 15**, in which none of the sorbents' peak reaction rates demonstrated a trend with temperature. If temperature seemingly had no effect on peak reaction rates of the sorbents, then perhaps the discrepancy in their magnitudes is due to the differences in initial porosity and physical structures of the sorbents. Because the CO_2 was being fed at such a high partial pressure, the product layer may have formed almost immediately, causing the entire carbonation period to be diffusion controlled. Other experiments analyzed by the RPM and run at CO_2 partial pressures of 5%-15% transition from the kinetically controlled region to the diffusion region at about three to five minutes (Zhou, Xu et al. 2013). From the experimental conversion trends presented earlier in **Figures 11-13**, and the parameter estimated switch times in **Table 3**, it can be seen that the kinetically controlled region lasts only about one to two minutes. In addition to this, the software reported a switch time of 10 seconds for the CaO-NF run at 600°C. At 650°C, the software could not generate a tight estimate for this parameter for the CaO-NF sorbent, claiming that the optimal switch time was 6 seconds with an interval of about 2 seconds. This may be due to the large surface area and low bulk density of the sorbent, combined with the high partial pressure of CO_2 reactant. These factors contribute to the extremely rapid carbonation of the sorbent, explaining the much smaller switch times. Despite the fact that the Athena software was able to generate reasonable switch time results at 700°C and 750°C, it should be noted that perhaps experiments run at a lower partial pressure of reactant may provide more accurate parameters.

Modeling Results and Discussion: Overlapping Grain Model

Equations 22-28 present a mixed set of ordinary differential equations and algebraic equations that were also inputted into Athena. As mentioned earlier, the only two input parameters

for the OGM are the initial porosity and the discretized grain size distribution of the sorbent particles. Because these input parameters were rough estimates from the literature, they may not be completely representative of the system at hand, but should provide a good enough foundation for future experimental work. Due to the nature of the experimental setup and the parameters within the OGM itself, the calculated model sometimes fails to capture some of the experimental trends. For this reason, the software cannot find an optimal k_{OGM} or D_{OGM} for the low performing runs, as the employed discrete grain distribution coupled with the large CO_2 partial pressure makes it impossible to minimize the residuals enough such that a solution is reached. Depending on the run being analyzed, the software either encounters undefined values during calculation and fails, or provides a non-acceptable solution, with k_{OGM} or D_{OGM} confidence intervals that are much larger than their optimal values. However, the software was able to compile and estimate parameters for some of the experimental runs. **Figure 20** depicts an example of a successful parameter estimation in which the model captures the features of the conversion trend.

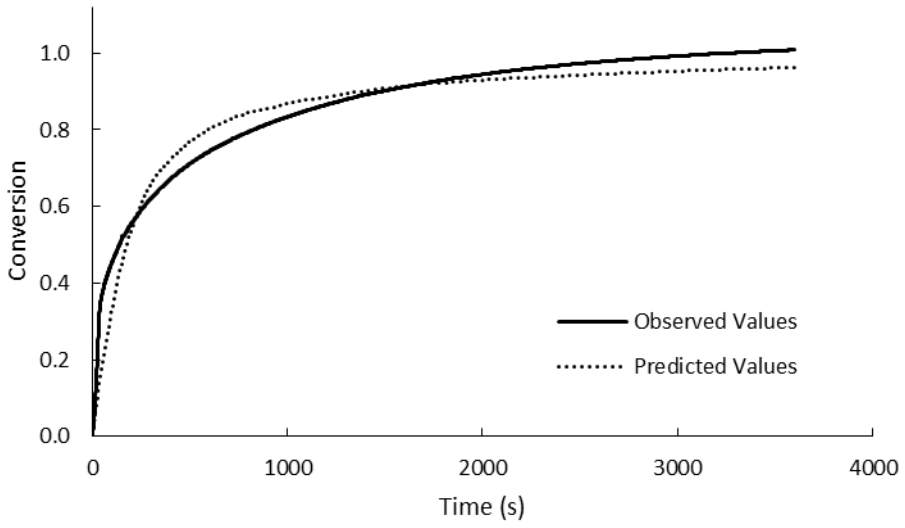

Figure 20. Athena parameter estimation output for the OGM, plotting conversion versus reaction time. The black data trend is from the experiment in which CaO-NF was carbonated under 200 mL/min of 100% CO_2 at 650°C. The grey data trend is the model calculated values.

The poor fit may be due to Athena finding a local minimum and using that as the optimal solution. To avoid this, perhaps better fitting initial conditions can be used, or loosening some of the optimization parameters to sweep more possible solutions. The model usually fails to find a solution because it cannot capture the steep shift in conversion. From the conversion trends in **Figure 11-13**, there is almost a discontinuity as the system very abruptly switches from a kinetically controlled region to diffusion controlled. In addition to this, the kinetically controlled regime is steep and short-lived, which are features that the OGM is not robust enough to emulate, at least with the parameters being used here. Efforts have been made to employ more accurate grain size distributions. It has been reported that a single grain size of 50nm is sufficient enough for the OGM to capture calcined limestone carbonation (Liu, Dennis et al. 2012). The CaO-CaAcetate sorbent's grain size distribution was also estimated from a plot depicting the particle size distribution of a calcium oxide sample derived from CaAcetate. Neither attempts yielded any successful results when they were tested on the CaO-Marble and CaO-CaAcetate runs. Another possible reason is that the OGM is simply incapable of modelling results at high partial pressures of reactant in this calcium oxide carbonation, as it has only been successfully tested in experimental setups in which CO_2 partial pressures ranged from only 5%-15% (Liu, Dennis et al. 2012, Zhou, Xu et al. 2013). Running at a lower partial pressure of CO_2 will extend the kinetically controlled carbonation period, making the shift much less abrupt. With this new, less steep conversion trend, perhaps the model will be able to fit the data with an acceptable trend.

Modeling Results and Discussion: Residuals

Residuals are the differences between a model's calculated values and the actual experimental data the model is being compared against. An indicator of a good model that

faithfully captures experimental data is if the system's residuals are unordered, and are randomly distributed throughout along the axis of the independent variable. If the residuals are unordered, then any discrepancy between the calculated model values and the experimental data is just a result of natural random variance. However, if the residuals are ordered, then the model is not faithfully emulating the physical process that is happening. **Figure 21** below is a plot of the residuals of the RPM for the CaO-Marble run at 650°C. It is clear that the residuals are highly ordered, meaning that the model is definitely not perfect, despite having a large R^2 value. Because the RPM is a piecewise function that separates the kinetically controlled region from the diffusion controlled region, it is useful to analyze the residuals within these two regions in an attempt to understand where and why the model fails to capture the data. A closer look at the residuals can be seen in **Figure 22**, in which the residuals for a single CaO-Marble run at 650°C is separated into the two distinct regions.

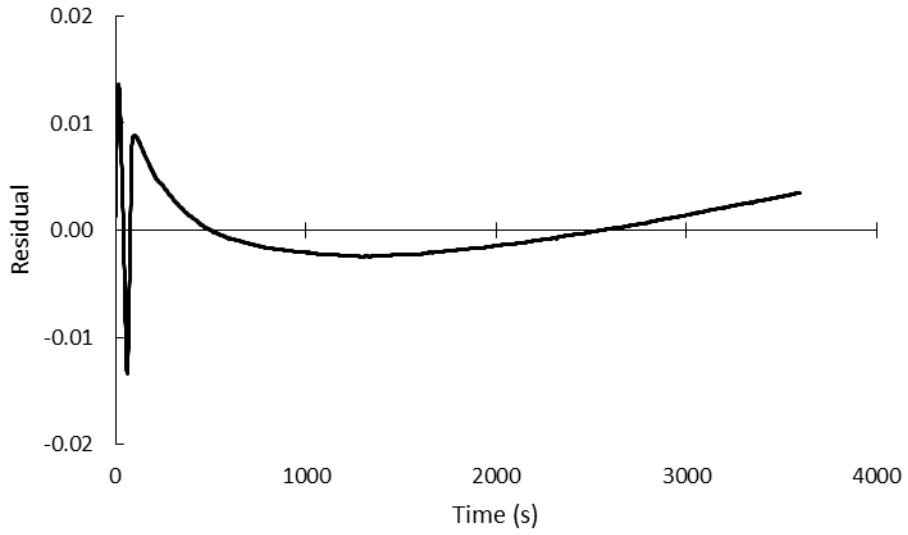

Figure 21. Residuals (Athena predicted values minus observed values) versus reaction time for the RPM. The experimental values were taken from a CaO-Marble sample, carbonated under 200 mL/min of 100% CO_2 at 650°C.

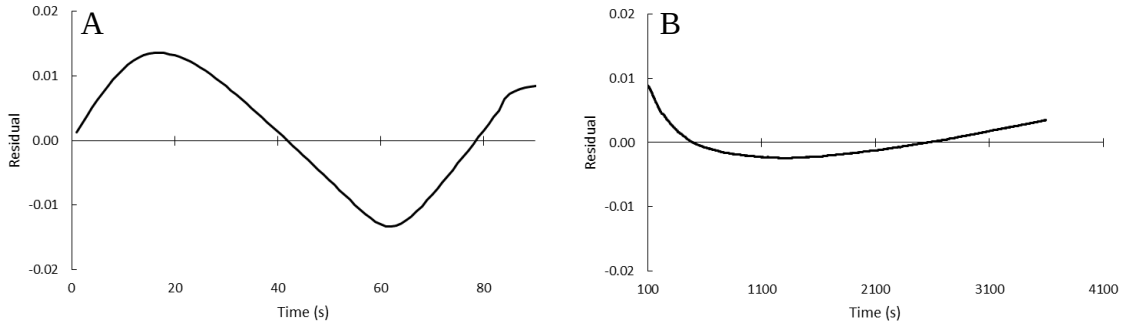

Figure 22. Residuals (Athena predicted values minus observed values) versus reaction time for the RPM. The experimental values were taken from a CaO-Marble sample, carbonated under 200 mL/min of 100% CO_2 at 650°C. The residuals are split into the first 80 seconds of carbonation, which is the kinetic region (A), and the rest of the carbonation period, which is the diffusion controlled region (B).

In the kinetic region, it looks like the model first overestimates the carbonation at the very start, and then underestimates it. This discrepancy is a possible artifact from the extremely steep carbonation in the first few seconds of the experiment. The model's linear dependence on time then cannot capture the apparent curvature in the data. In the diffusion controlled region, the residuals are highly ordered as well. During the first few minutes of carbonation in this region, the model greatly overestimates the curve, before dipping and underestimating the data. Finally the model continues to overestimate the trend, as conversion levels off to some equilibrium value in the physical system. This again highlights the fact that the model's simple dependence on time is not sufficient enough to capture the curvature. In the real physical system at hand, conversion is clearly not a simple square root of time dependence. Plotting the residuals for the other runs and at other temperatures provides the same residual pattern. **Figure 23** plots the residuals from the three precursors run at 700°C, to get an idea of the magnitude of the discrepancies.

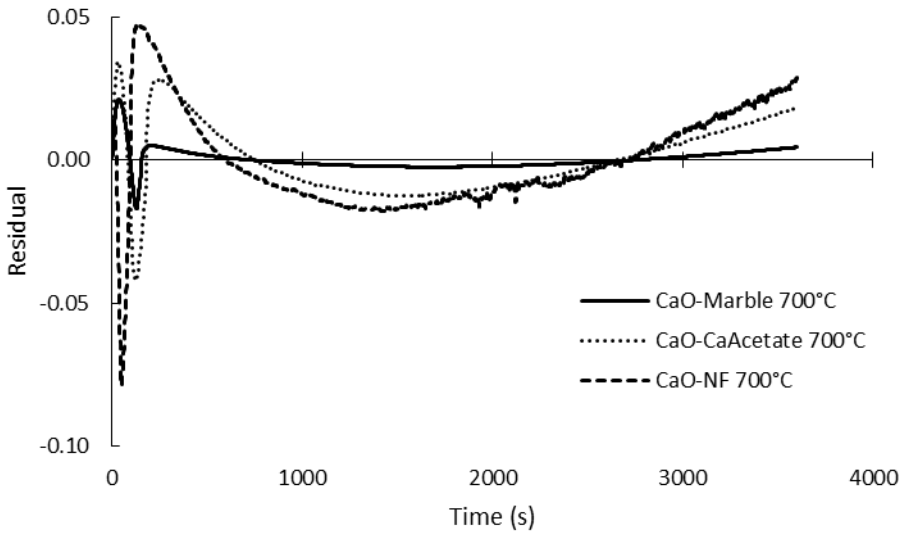

Figure 23. Residuals (Athena predicted values minus observed values) versus reaction time for the RPM. The experimental values were taken from CaO-Marble, CaO-CaAcetate, and CaO-NF experiments, in which the sorbents were carbonated under 200 mL/min of 100% CO_2 at 700°C.

The residuals from the OGM can be plotted as well, to see how closely the model fits to the data. These residuals are plotted in **Figure 24**, for the CaO-NF run at 650°C. Interestingly enough, the OGM residuals exhibit a different trend from the RPM. The model severely underestimates the early conversion present in the kinetically controlled region. Again, the steep carbonation of the sorbent is not being captured by the model, as the OGM cannot model this rapid weight gain. The model then overestimates during the early portion of the diffusion controlled region. This overestimation is necessary to minimize the residuals during the later portions of the diffusion controlled region.

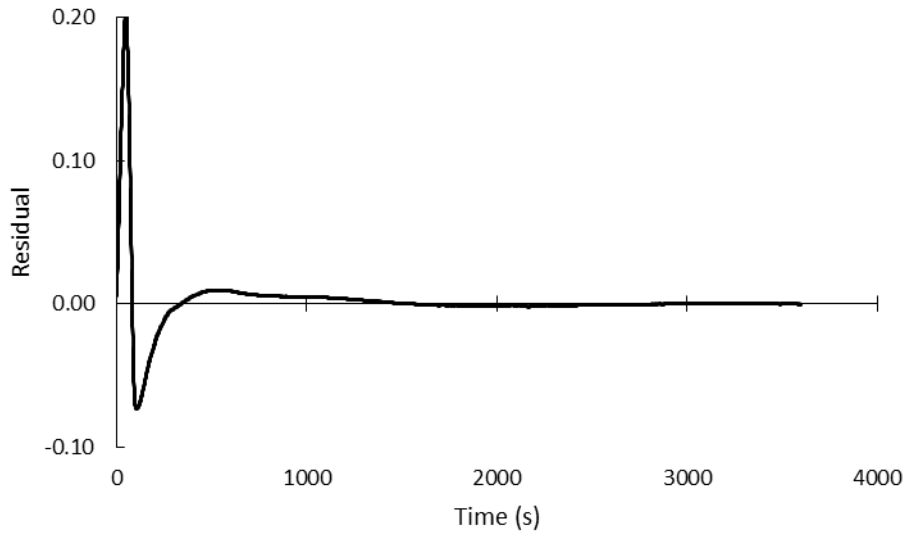

Figure 24. Residuals (Athena predicted values minus observed values) versus reaction time for the OGM. The experimental values were taken from a CaO-NF sample, carbonated under 200 mL/min of 100% CO_2 at 700°C.

From **Figure 23** and **Figure 24**, it can be seen that the magnitude of the residuals are larger in the OGM, at least in this case. This indicates that the RPM is a better model of the system at hand, and that it more closely emulates the experimental data, although it should be noted that the OGM seems to capture the end of the carbonation period quite well. Overall however, the RPM seems to provide a much better fit, as can be seen in **Figures 16 – 17**, and **Figure 20**. Due to the nature of the reaction at hand, it makes sense as to why the RPM fits the data more closely than the OGM. The RPM is a piecewise function, and the carbonation of calcium oxide almost exhibits a discontinuity which is further enhanced by the fact that the experiments were run under 100% CO_2. A piecewise function allows for a more flexible model that can choose the optimal time to switch between the appropriate functions. The OGM on the other hand, is a more traditional continuous differential equation system, and will have difficulty attempting to model experimental data that exhibits such sharp shifts in trends. However, the simple square root of time dependence

present in the RPM fails to capture the behavior at longer carbonation times, in which the conversion tapers off to a horizontal line.

Conclusions

The carbonation of calcium oxide has been proven to be an extremely important reaction to study in the context of steam methane reforming. The work presented here is an attempt to lay a foundation for the analysis of calcium oxide sorbents derived from various precursors. By using thermogravimetric analysis, conversion trends and reaction rates can be calculated. It was shown that vendor supplied calcium oxide derived from marble is not a homogeneous sample, as different samples' carbonation behavior varied wildly. Pretreating the sample seemed to have no effect on carbonation kinetics, but it did seem that the older, more aged samples experienced slightly higher reaction rates. Calcium oxide sorbents were derived from marble (CaO-Marble), calcium acetate (CaO-CaAcetate), and electrospun composite nanofibers (CaO-NF) and were compared with each other, with the CaO-NF sorbent performing much better than its other two counterparts in a temperature range of 600°C-800°C.

These conversion trends were then compared to physical models found in the literature, showing that parameter estimation is possible for the system. The random pore mode (RPM) fit the experimental data more closely than the overlapping grain model (OGM) did, and seemed to be more robust as well. Due to its simplicity, the RPM was easily applied to all of the runs, while the OGM encountered a few difficulties such that a solution could not be found. Kinetic rate constants and diffusivities were compared and contrasted between the precursors, demonstrating the usefulness of these physical models. An analysis of the residuals confirmed that neither of the two models fully captured all of the trends in the experimental data. However, their usefulness

should not be understated, as this analysis can still provide a powerful quantitative tool to compare and contrast the performance of sorbents of interest.

The structural parameters used for the software here provide only rough estimates. To obtain their true values, chemical analysis must be conducted on the samples, providing a much more accurate model, leading to much more accurate kinetic rate constants and diffusivities in the parameter estimation process. It is clear that the time scale between the two distinct regions are very different. The kinetically controlled region is on the order of a few minutes, while the diffusion controlled region can potentially be up to a few hours, depending on the experimental setup. However, as it stands in the software, every data point has equal weight in calculating the optimal parameters. This may be skewing the results as it is putting much greater weight on the diffusion controlled region, due to its much larger number of data points compared to the kinetic region. More accurate parameters can be estimated if the weight of the data points in the kinetically controlled region was increased such that it is at least equal to the diffusion controlled region. Future work in this field can include the chemical analysis of the sorbent after it has fully carbonated, to ensure the product is completely calcium carbonate. As shown earlier, the CaO-NF exhibited conversions greater than 100%, and it would be useful to see exactly what is being formed, assuming this anomaly is not due to instrument or process error. Running at a lower partial pressure of CO_2 may be helpful as well. By decreasing the reactant concentration, the kinetic region of the carbonation reaction can be elongated. This can potentially lead to more accurate parameters during the parameter estimation process, as both presented models may fit the data more closely, and perhaps an Arrhenius relationship can be observed for the kinetic rate constant.

Another important facet to consider is sorbent cycling, in which the experiment is designed to test sorbent performance during multiple carbonation and calcination cycles. Because this is a

reaction run on an industrial scale, the process economics must always be kept in consideration. If it can be shown that calcium oxide derived from electrospun nanofibers are more stable than their marble counterparts during many cycles of usage, the impact would be significant. Their excellent performance has already been exhibited, and they have the potential to become a much more economical choice, providing a much needed alternative.

References

Albrecht, K. O., et al. (2010). "Application of a combined catalyst and sorbent for steam reforming of methane." Industrial & Engineering Chemistry Research **49**(9): 4091-4098.

Avrami, M. (1940). "Kinetics of phase change. II transformation-time relations for random distribution of nuclei." The Journal of Chemical Physics **8**(2): 212-224.

Barelli, L., et al. (2008). "Hydrogen production through sorption-enhanced steam methane reforming and membrane technology: a review." Energy **33**(4): 554-570.

Bhatia, S. and D. Perlmutter (1981). "A random pore model for fluid-solid reactions: II. Diffusion and transport effects." AIChE Journal **27**(2): 247-254.

Bhatia, S. and D. Perlmutter (1983). "Effect of the product layer on the kinetics of the CO2-lime reaction." AIChE Journal **29**(1): 79-86.

Bhatia, S. K. and D. Perlmutter (1980). "A random pore model for fluid-solid reactions: I. Isothermal, kinetic control." AIChE Journal **26**(3): 379-386.

Formo, E., et al. (2008). "Functionalization of electrospun TiO2 nanofibers with Pt nanoparticles and nanowires for catalytic applications." Nano Letters **8**(2): 668-672.

Grasa, G., et al. (2009). "Application of the random pore model to the carbonation cyclic reaction." AIChE Journal **55**(5): 1246-1255.

Grasa, G. S. and J. C. Abanades (2006). "CO2 capture capacity of CaO in long series of carbonation/calcination cycles." Industrial & Engineering Chemistry Research **45**(26): 8846-8851.

Huang, Z.-M., et al. (2003). "A review on polymer nanofibers by electrospinning and their applications in nanocomposites." Composites science and technology **63**(15): 2223-2253.

Li, Z.-s., et al. (2012). "Effect of temperature on the carbonation reaction of CaO with CO2." Energy & Fuels **26**(4): 2473-2482.

Liu, W., et al. (2012). "An investigation of the kinetics of CO 2 uptake by a synthetic calcium based sorbent." Chemical engineering science **69**(1): 644-658.

Lu, H., et al. (2006). "Calcium oxide based sorbents for capture of carbon dioxide at high temperatures." Industrial & Engineering Chemistry Research **45**(11): 3944-3949.

Manovic, V. and E. J. Anthony (2007). "Steam reactivation of spent CaO-based sorbent for multiple CO2 capture cycles." Environmental science & technology **41**(4): 1420-1425.

Morales-Flórez, V., et al. (2015). "Hydration and carbonation reactions of calcium oxide by weathering: Kinetics and changes in the nanostructure." Chemical Engineering Journal **265**: 194-200.

Perraki, T. and A. Orfanoudaki (2004). "Mineralogical study of zeolites from Pentalofos area, Thrace, Greece." Applied Clay Science **25**(1): 9-16.

Silaban, A., et al. (1992). "Calcium acetate as a sorbent precursor for the removal of carbon dioxide from gas streams at high temperature." Resources, conservation and recycling **7**(1-3): 139-153.

Sotirchos, S. V. (1987). "On a class of random pore and grain models for gas-solid reactions." Chemical engineering science **42**(5): 1262-1265.

Sotirchos, S. V. and H. C. Yu (1988). "Overlapping grain models for gas-solid reactions with solid product." Industrial & Engineering Chemistry Research **27**(5): 836-845.

Thavasi, V., et al. (2008). "Electrospun nanofibers in energy and environmental applications." Energy & Environmental Science **1**(2): 205-221.

Zhou, Z., et al. (2013). "Modeling of the carbonation kinetics of a synthetic CaO-based sorbent." Chemical engineering science **95**: 283-290.